iScience

CellPress

Article

Toward an MRI-Based Mesoscale Connectome of the Squid Brain

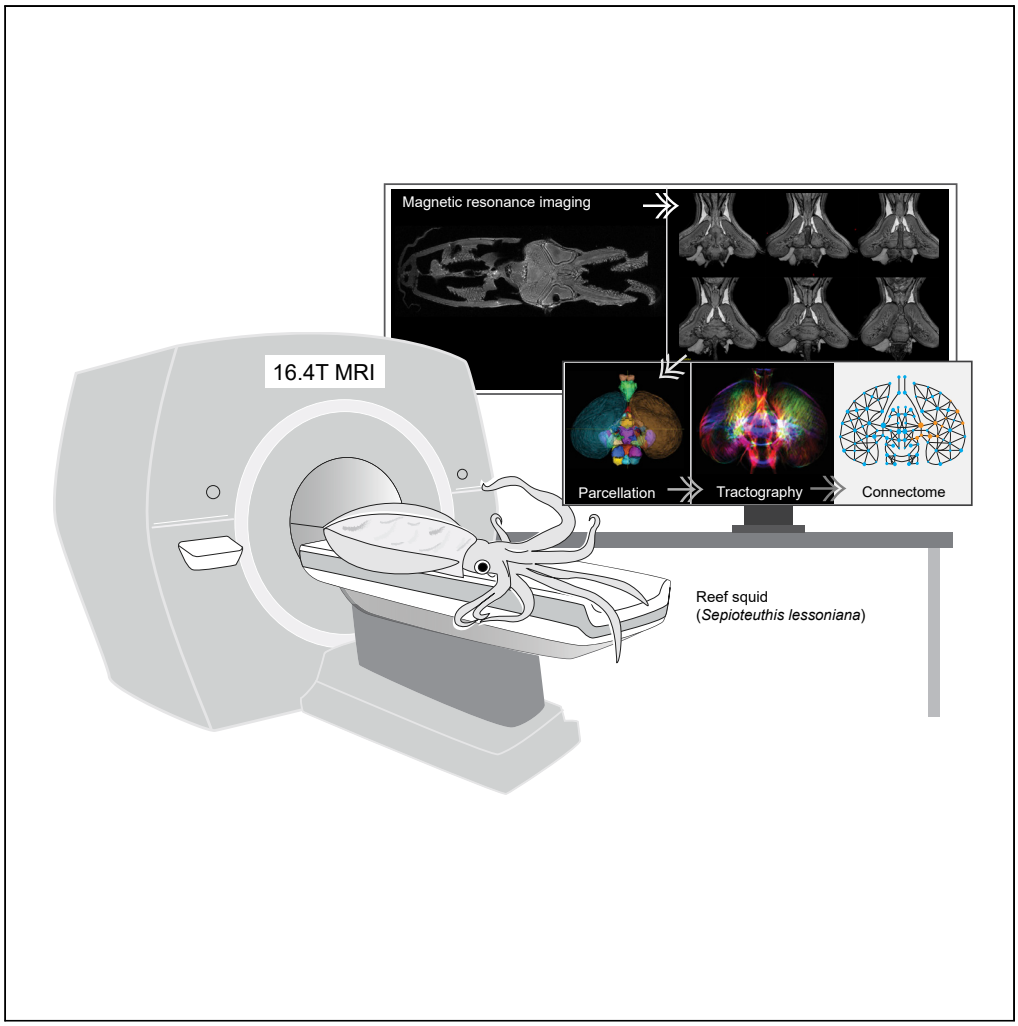

Wen-Sung Chung, Nyoman D. Kurniawan, N. Justin Marshall

w.chung1@uq.edu.au (W.-S.C.)
justin.marshall@uq.edu.au (N.J.M.)

HIGHLIGHTS

The first MRI-based connectome in a cephalopod

Retinotopic organization through the optic lobes and into other brain areas

Subdivided basal lobe system defines topographic information from optic lobes

A new chiasm is proposed to coordinate vision and countershading camouflage

Chung et al., iScience *23*, 100816
January 24, 2020
https://doi.org/10.1016/j.isci.2019.100816

iScience

CellPress

Article

Toward an MRI-Based Mesoscale Connectome of the Squid Brain

Wen-Sung Chung,[1,3,*] Nyoman D. Kurniawan,[2] and N. Justin Marshall[1,*]

SUMMARY

Using high-resolution diffusion magnetic resonance imaging (dMRI) and a suite of old and new staining techniques, the beginnings of a multi-scale connectome map of the squid brain is erected. The first of its kind for a cephalopod, this includes the confirmation of 281 known connections with the addition of 145 previously undescribed pathways. These and other features suggest a suite of functional attributes, including (1) retinotopic organization through the optic lobes and into other brain areas well beyond that previously recognized, (2) a level of complexity and sub-division in the basal lobe supporting ideas of convergence with the vertebrate basal ganglia, and (3) differential lobe-dependent growth rates that mirror complexity and transitions in ontogeny.

INTRODUCTION

Cephalopods have the most complicated central nervous system (CNS) of all invertebrates at both anatomical and functional levels as demonstrated by the pioneering neuroanatomical work of Cajal and Young decades or indeed a century ago (Cajal, 1917; Young, 1961, 1971, 1974, 1976, 1977, 1979). The brains of all coleoid cephalopod groups (octopus, cuttlefish, and squid but not nautilus) are built around a circumesophageal set of ganglia or lobes that have expanded dramatically (Figures 1 and S1 and Videos S1 and S2). In particular, their complex visual system and limb-based tactile capability set the cephalopods apart from other molluscs (Figure 1) (Wells and Wells, 1957; Bullock and Horridge, 1965; Nixon and Young, 2003; Chung and Marshall, 2014; Liu and Chiao, 2017; Shigeno et al., 2018). Early work on the organization of the cephalopod sensory and motor control systems combined with comparative studies in behavioral changes before and after brain-region ablation suggested a useful model for studying sensory function, learning, and memory (Boycott and Young, 1955, 1957; Wells and Wells, 1957; Boycott, 1961, 1965; Young, 1971, 1974, 1976, 1977, 1979; Messenger, 1979; Abbott et al., 1995). Based on distinct morphological and functional features, the coleoid cephalopod brain can be divided into four major divisions: (1) the vertical lobe complex (learning and memory); (2) a pair of optic lobes (vision-related tasks); (3) supraoesophageal mass (higher motor control centers coordinating sensory inputs and behavioral responses); (4) suboesophageal mass (lower motor control centers executing simple movement of fins and arms, and mantle activities for respiration) (Video S2). A detailed list of categories of sub-regions within the lobe systems can be found in Table 1. However, more recent model systems in neuroscience have moved away from the cephalopods and, with few exceptions, their functional neuroanatomy has languished (Boycott, 1961; Miyan and Messenger, 1995; Brown et al., 2006; Zullo et al., 2009; Liu and Chiao, 2017; Shomrat et al., 2008).

By contrast, several studies have focused on the behavioral neurobiology of the cephalopods and their remarkably rapid and apparently smart reactions to novel challenges. Such behaviors suggest that the coleoids at least have developed alternative ways of problem solving compared with standard model species such as mice, zebrafish, and fruit flies (Darmaillacq et al., 2014; Bublitz et al., 2017; Liscovitch-Brauer et al., 2017; Hanlon and Messenger, 2018; Schnell and Clayton, 2019). Most famous cases in this respect are the remarkable color-blind camouflage, mimicry, and other communication abilities that they are capable of (Marshall and Messenger, 1996; Chung and Marshall, 2016; Lin et al., 2017; How et al., 2017; Hanlon and Messenger, 2018). Other studies reveal the richness of cephalopod behavioral repertoires (e.g., pattern recognition, bipedal walking, mate guarding, social cognition, and observational learning) and suggest that some instances are comparable with the abilities of higher vertebrates (Sutherland et al., 1963; Fiorito and Scotto, 1992; Darmaillacq et al., 2014; Bublitz et al., 2017; Hanlon and Messenger, 2018; Schnell and Clayton, 2019). Interestingly, some of these studies suggest that a somatotopic relationship from brain to the outside world is lacking (Zullo et al., 2009; Liu and Chiao, 2017), but results we present here as

[1]Queensland Brain Institute, The University of Queensland, St Lucia, QLD 4072, Australia

[2]Centre for Advanced Imaging, The University of Queensland, St Lucia, QLD 4072, Australia

[3]Lead Contact

*Correspondence: w.chung1@uq.edu.au (W.-S.C.), justin.marshall@uq.edu.au (N.J.M.)

https://doi.org/10.1016/j.isci.2019.100816

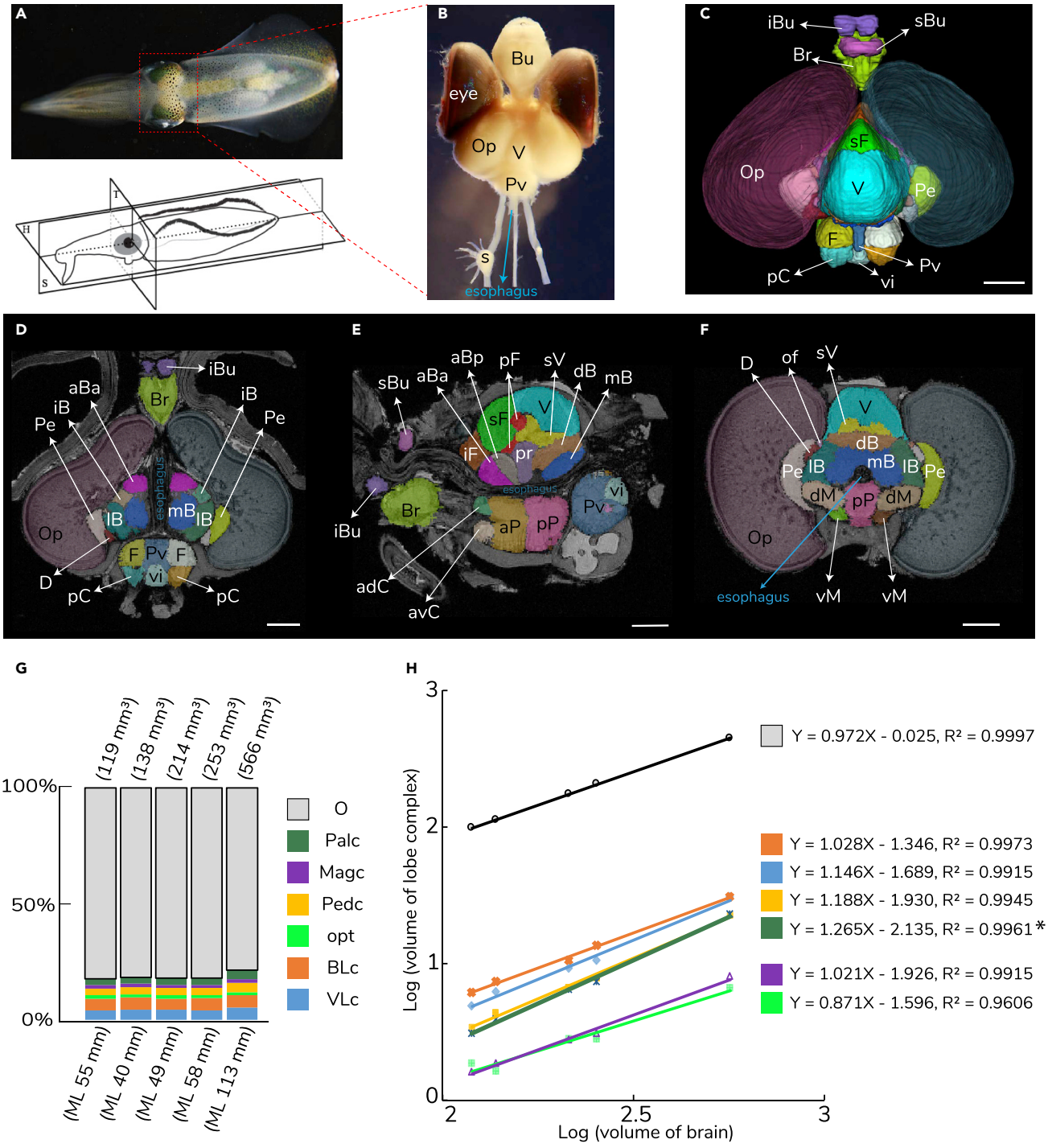

Figure 1. Squid (*Sepioteuthis lessoniana*) Multi-lobed Brain

A juvenile reef squid brain.

(A) Close-up of squid head. Live specimen (dorsal view) and a schematic drawing represents three anatomical planes.

(B) Isolated squid brain and eyes. Bu, buccal mass; Op, optic lobe; Pv, palliovisceral lobe; s, stellate ganglion; V, vertical lobe.

(C) MRI-based 3D reconstruction of squid multi-lobed brain. Br, brachial lobe; F, fin; iBu, inferior buccal; pC, posterior chromatophore; Pe, peduncle; sBu, superior buccal; sF, superior frontal; vi, visceral.

(D–F) Parcellation of the squid brain derived by anatomical landmarks. (D) Sagittal section. (E) Transverse section. (F) Horizontal section. aBa, Anterior basal lobe; adC, anterior dorsal chromatophore; aBp, anterior posterior basal; aP, anterior pedal; avC, anterior ventral chromatophore; dB, dorsal basal; dM,

Figure 1. *Continued*

dorsal magnocellular; D, dorsolateral; iB, interbasal; iF, inferior frontal; lB, lateral basal; mB, median basal; pP, posterior pedal; pF, posterior frontal; pr, precommisural; sV, subvertical; vM, ventral magnocellular. Scale bar: 1 mm.

(G) Brain volume and percentage of each lobe complex volume in five squid individuals. Owing to partial damage of brachial and buccal lobes in two specimens, the brain volume excludes the brachial lobe complex. ML, mantle length. Color-coded symbols represent the lobe complex as: BLc, basal lobe complex; Magc, magnocellular lobe complex; O, optic lobes; opt, optic track complex; Palc, palliovisceral lobe complex; Pedc, pedal lobe complex; VLc, vertical lobe complex. Detailed volumetric data can be found in Table S1. All abbreviations also in Table 1.

(H) Allometric analysis of the lobe complex. Color-coded regression line for each lobe complex showing significant variance of the slopes among seven regression lines (ANOVA, df = 6, $p < 0.0001$). In particular, the palliovisceral lobe complex volume scales with positive allometry (slope 1.2645) and with a 95% confidence interval around the slope (1.1167–1.4124) excludes 1 (isometry), indicating that this lobe complex grows disproportionately and its disproportionality increases with increased volume of the brain.

See also Figure S1 and Table S1.

well as recent suggestions from others (Grasso, 2014; Shigeno et al., 2018) suggest that this visual world to motor output does exist.

Despite intense interest and research progress concerning cephalopod complex behavioral and cognitive abilities, even for the common octopus, *Octopus vulgaris*, which is the most well-studied species (Boycott and Young, 1955, 1957; Young, 1961, 1971; Sutherland et al., 1963; Fiorito and Scotto, 1992; Nixon and Young, 2003; Shomrat et al., 2008; Zullo et al., 2009; Wollesen et al., 2012; Darmaillacq et al., 2014), understanding its brain-wide neural network and the associated functional circuits remains incomplete. Our current knowledge of cephalopod nervous systems is derived from multiple levels and may be summarized in the following categories: (1) decoding the genomic sequence (Albertin et al., 2015; Liscovitch-Brauer et al., 2017; Edsinger and Dölen, 2018); (2) molecular and synaptic activities (Shomrat et al., 2008; Wollesen et al., 2012; Lee et al., 2013; Shigeno and Ragsdale, 2015; Edsinger and Dölen, 2018); (3) electrophysiological studies (Miyan and Messenger, 1995; Chrachri and Williamson, 1998; Shomrat et al., 2008; Hu et al., 2009; Zullo et al., 2009; Liu and Chiao, 2017); (4) gross neural anatomy and connectivity using classical histology (Cajal, 1917; Young, 1971, 1974, 1976, 1977, 1979; Messenger, 1979; Maddock and Young, 1987; Shigeno et al., 2001; Nixon and Young, 2003; Wollesen et al., 2009; Kobayashi et al., 2013; Wild et al., 2015; Koizumi et al., 2016); (5) magnetic resonance imaging (MRI) of the brain (Chung and Marshall, 2014, 2017; Liu et al., 2018). It is in this latter category, using modern neuroanatomical techniques, that we aim to contribute toward describing new neural pathways and the behaviors they mediate, and we start with the reef squid, *Sepioteuthis lessoniana*. This loliginid species has been studied extensively in terms of its sensory ecology and behavior making it a suitable first subject (Hu et al., 2009; Sugimoto and Ikeda, 2012; Chung and Marshall, 2014, 2016; Lin et al., 2017; Lin and Chiao, 2017; Liu and Chiao, 2017; Lu and Chung, 2017). It is also closely related to previously studied loliginid squid species (Anderson, 2000; Messenger, 1979; Strugnell et al., 2005; Vecchione et al., 1998; Young, 1974, 1976, 1977, 1979), allowing confidence in the cross-species comparisons made here between old and new methods. Descriptions of cuttlefish, coastal benthic octopuses, and vampire squid brain connectomes using similar techniques are ongoing.

One major challenge in mapping any brain is in the untangling of inter-woven neural fibers into the discrete bundles related to specific functional circuits rather than those that are simply anatomically concomitant. With this in mind, three long-standing problems have produced variable results in cephalopods: the inconsistent stochastic nature of silver staining methods, practical difficulties in examining a large-sized brain, and the methodological constraint of classical histology to a single section angle per specimen (Young, 1974, 1976, 1977, 1979; Messenger, 1979; Valverde, 1998).

The large-scale, unfamiliar mollusc plan and neuronal diversity of cephalopods make a synapse-level wiring diagram unlikely in the near future. For other invertebrates with smaller brains, such as *Drosophila* and nematode worms, these detailed connectomes are becoming reality (Cook et al., 2019; Meinertzhagen, 2018; Shih et al., 2015; Takemura et al., 2017; White et al., 1986) and are an important first step in understanding function and cognition in any animal. The brain of a mouse, which is around the same size as the squid used in this study, now has what is described as a complete connectome at mesoscale (Oh et al., 2014; Liu et al., 2016). The mouse Allen Brain Atlas (ABA) is based on a huge quantity of histological and neuronal tracing data and is now beginning to be supported by cross comparisons with high-resolution (9.4 and 16.4 Tesla) MRI (Calamante et al., 2012; Kurniawan et al., 2014; Calabrese et al., 2015; Liu et al., 2016) as well as serial block face electron microscopy (Deweerdt, 2019). The same basic cross-correlative

Lobe System and Function	Lobe	Abbreviation
Vertical lobe complex (VLc)—memory and learning	Inferior frontal	iF
	Superior frontal	sF
	Posterior frontal	pF
	Subvertical	sV
	Vertical	V
Basal lobe complex (BLc)—higher motor control	Anterior anterior basal	aBa
	Anterior posterior basal	aBp
	Precommisural	pr
	Dorsal basal*	dB
	Interbasal*	iB
	Median basal	mB
	Lateral basal*	lB
Optic track complex (opt)—intermediate visual-motor center and olfaction	Peduncle*	Pe
	Olfactory*	of
	Dorsolateral*	D
Brachial lobe complex (Brc)—arm and feeding control	Inferior buccal	iBu
	Superior buccal	sBu
	Brachial	Br
Pedal lobe complex (Pedc)—intermediate and lower motor center for locomotion control	Anterior dorsal chromatophore* $^{\Psi}$	adC
	Anterior ventral chromatophore* $^{\Psi}$	avC
	Anterior pedal	aP
	Lateral pedal*	lP
	Posterior pedal	pP
Magnocellular lobe complex (Magc)—intermediate motor center	Dorsal magnocellular*	dM
	Ventral magnocellular*	vM
	Posterior magnocellular*	pM
Palliovisceral lobe complex (Palc)—lower motor center for locomotion and mantle activities	Palliovisceral	Pv
	Lateral ventral palliovisceral*	lvP
	Fin*	F
	Posterior chromatophore*	pC
	Visceral	vi
Optic lobes (O)—vision	Optic*	Op

Table 1. List of Squid Brain Lobes with Abbreviations Used through the Text

The main functions of the lobe systems based on work by Young and his colleagues (Messenger, 1979; Young, 1961, 1971; 1974, 1976; 1977, 1979; Boycott and Young, 1955, 1957; Wells and Wells, 1957; Nixon and Young, 2003). Supraoesophageal mass includes basal lobe and optic track complexes. Suboesophageal mass consists of the brachial lobe, pedal lobe, magnocellular lobe, and palliovisceral lobe complexes. * indicates that the lobe is further divided into the left and right lobe. $^{\Psi}$ indicates a further sub-division of the anterior chromatophore lobes into dorsal and ventral halves.
(See also Figures 1 and S1).

ideas are applied here to map and model the elements and potential interactions of the squid brain (Bullmore and Sporns, 2009; Bassett and Sporns, 2017; Assaf et al., 2019). As noted in mouse and other vertebrate work (Jbabdi and Johansen-Berg, 2011; Donahue et al., 2016; Maier-Hein et al., 2017; Aydogan et al., 2018; Suarez et al., 2018; Sotiropoulos and Zalesky, 2019), several caveats should be applied to probabilistic MRI-based tractography, and it is often best viewed as supportive and predictive rather than a fully validated functional connectome.

Several morphological and methodological factors detailed below allow a closer correlation and greater confidence of anatomical accuracy from pathways predicted from MRI projections alone in squid compared with those in mouse. First, the invertebrate nervous systems share a more similar layout between individuals than the vertebrates (Bullock and Horridge, 1965; Young, 1974, 1976, 1977, 1979; Messenger, 1979; Nixon and Young, 2003; Strausfeld, 2005; Strausfeld et al., 2016; Suarez et al., 2018). Also, organization of brain lobes and the known underlying connections share a high degree of similarity across close phylogenetic groups (e.g., cuttlefish and squid) (Cajal, 1917; Boycott, 1961; Young, 1974, 1976, 1977, 1979; Messenger, 1979; Nixon and Young, 2003; Wild et al., 2015). Therefore, structural features, including individual cells and wiring patterns, may be reliably identified and re-visited between individuals or indeed between species and used to predict function. In addition, the higher signal-to-noise ratio and long scan time in the 16.4 T MRI (compared with 9.4 T) and highly conservative acceptance threshold (detail in Methods) that we use bring the scale of MRI and direct anatomical methods closer than in previous studies (Calamante et al., 2012; Kurniawan et al., 2014; Alomair et al., 2015; Ziegler et al., 2018). Combined with congruence of both previous (Cajal, 1917; Young, 1974, 1976, 1977, 1979; Messenger, 1979) and the current study and anatomical tract data with MRI-predicted projections, we may be more confident that the new regional interconnections proposed here are real.

Connectomes and brain maps confirm known functional interactions and where detailed enough may also predict function (Jbabdi and Johansen-Berg, 2011; Jbabdi et al., 2013; Shih et al., 2015; Meinertzhagen, 2018). Our findings in squid and possible new neuronal functions that they suggest may be summarized as follows:

(1) A similar number of lobes were found using MRI as by the traditional serial sectioning techniques of, e.g., Young (Young, 1974, 1976, 1977, 1979; Nixon and Young, 2003), but MRI delineated these much more clearly, allowing more accurate volumetric analysis to define differentials of lobe growth rate (Figures 1, S1, Tables 1, and S1).

(2) Tractography from five individuals combined with over 1,000 silver-stained sections and fluorescent neural tracers defined 145 new major pathways in the brain along with 99.65% of the previously known ones (Figures 2, 3, 4, and 5).

(3) Differentials of lobe growth and increasing complexity of the underlying neural network during growth mirror the sophisticated behavior repertoires that emerge during ontogeny (Figures 1G and 1H, 5D, S1, and Table S1).

(4) New aspects of spatial organization were uncovered in the optic lobes, including a preservation of retinotopicity to deeper layers than previously known. This topographic information could also project through to the basal lobe system (Figures 6 and 7 and Video S5).

(5) Within the basal lobe system, a new network of sub-divisions and interconnections was elucidated, probably coordinating visual and motor activity such as color change and body orientation (Figures 5, 6, 7, and 8). This provides another example of convergent evolution between cephalopods and vertebrates and supports recent hypotheses around a common brain-to-body bauplan convergence in many animals (Shigeno et al., 2018).

(6) A previously undescribed second chiasm between the lateral basal lobe and the anterior chromatophore lobes reorients the visual scene to the chromatophore display (Figures 8C–8E). This may enable coordination of camouflage and communication in body patterning.

It is worth underlining that, although MRI-based tractography has previously attracted a great deal of criticism (Thomas et al., 2014; Maier-Hein et al., 2017; Aydogan et al., 2018; Sotiropoulos and Zalesky, 2019), the methods and cross-checks applied here enable us to suggest that all new tracts proposed are valid (and

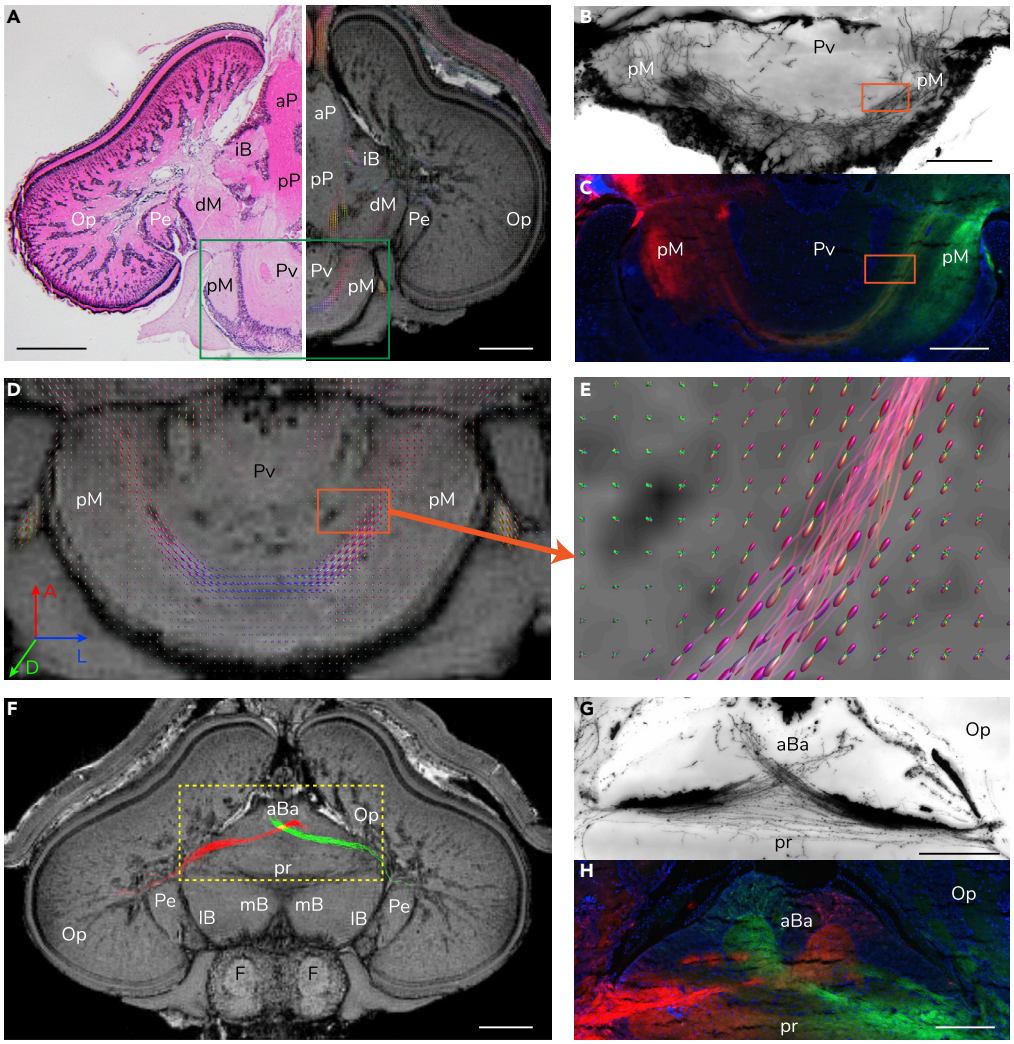

Figure 2. Cross-validation of the Squid Neural Tracts

(A) A comparison between conventional histology (left) (10-μm slice stained with hematoxylin and eosin) and magnetic resonance histology (right) (isotropic resolution 30 μm). The green rectangle indicates the posterior suboesophageal mass.

(B–E) An example of well-matched fiber orientation distribution (FOD) of neural tracts (orange rectangles) of the posterior magnocellular lobe (pM), which were validated among (B) Cajal-Golgi impregnation (40-μm slice), (C) fluorescent lipophilic dye tracers (25-μm slice), and (D) FOD. (E) A close-up of FOD and the corresponding streamlines (probabilistic tractography of the right pM), which were reconstructed using the optimized algorithm and acceptance criteria. The direction-encoded colors indicate orientation of body axis. A, anterior; D, dorsal; L, lateral.

(F–H) A sample of the matched neural tracts derived from two small regions of interest (each ROI voxel = 120 μm × 120 μm × 120 μm) in the anterior-median lobule of the anterior basal lobe (aBa) among (F) probabilistic tractography, (G) Cajal-Golgi impregnation (40-μm slice), and (H) fluorescent stained contralateral tracts (25-μm slice). Scale bar: 1 mm.

See also Figures S2 and S3.

see Calabrese et al. [2015]). Specifically, in a comparison with the previously known 282 squid neural tracts described by Young and his colleague (Young, 1974, 1976, 1977, 1979; Messenger, 1979), 281 were re-found using the high angular resolution diffusion-weighted imaging (HARDI) method combined with an ultra-conservative level for tractography acceptance employed here. In addition, only 36% of the new tracts proposed remain prediction-only with 64% confirmed through numerous Golgi impregnations or NeuroVue dye. Finally, long-scan-time 16.4 T resolution moves beyond general tract tracing and is closer to the scale of the individual neuron bundle at around 80 μm, reducing false positives and loss of tracing route.

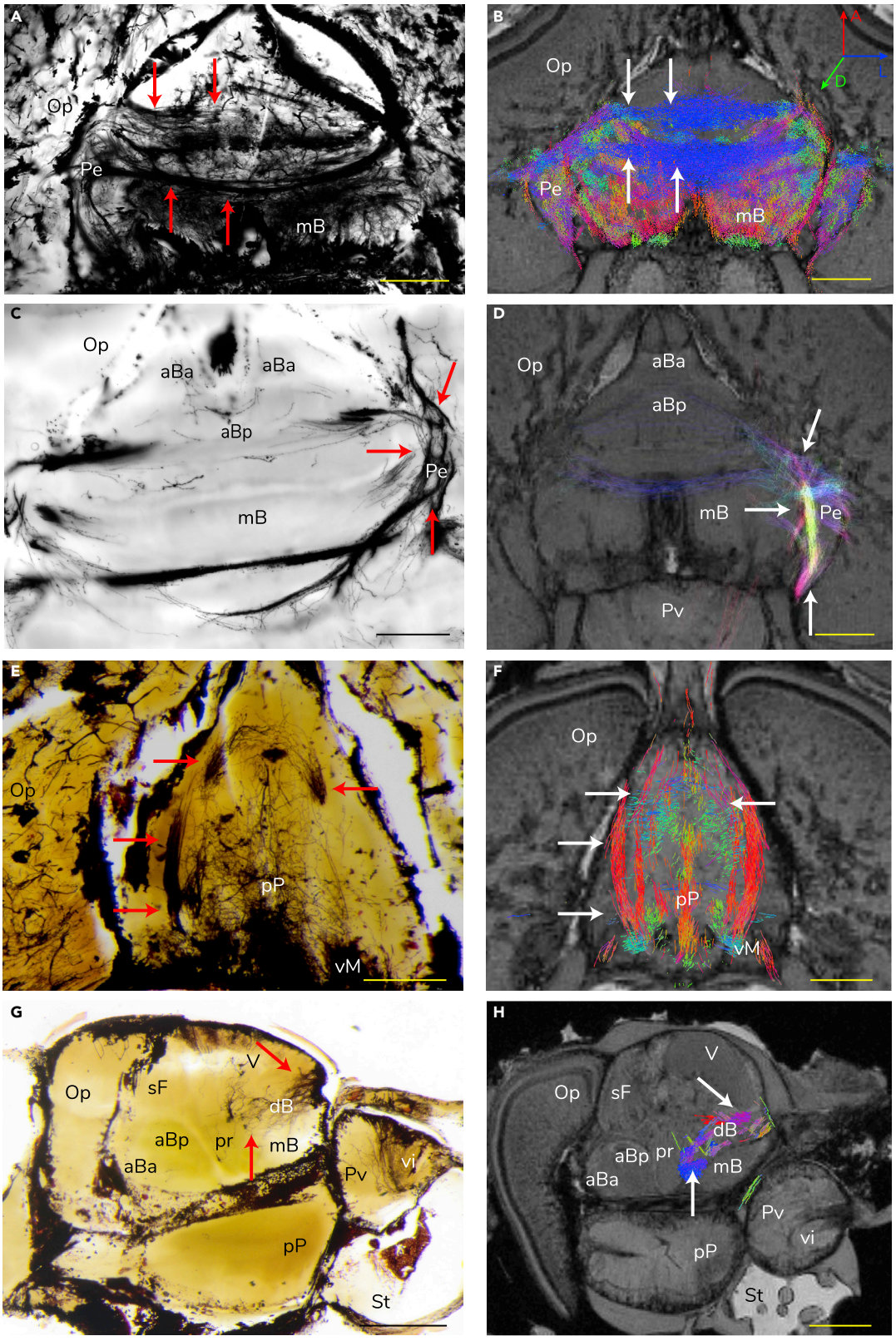
A
Op
Pe
mB
B
Op
A
L
D
Pe
mB
C
Op
aBa
aBa
aBp
Pe
mB
D
Op
aBa
aBp
mB
Pe
Pv
E
Op
pP
vM
F
Op
pP
vM
G
Op
sF
V
dB
aBp
pr
mB
aBa
Pv
vi
pP
St
H
Op
sF
V
dB
aBp
pr
mB
aBa
Pv
vi
pP
St

Figure 3. Comparisons of the Squid Neural Tract Counterparts between the Cajal-Golgi Impregnation and Tractography

Four pairs of examples showed the well-matched major tracts between two methods. Red arrows indicate silver stained neural bundles and white arrows indicate the tractographic counterparts. The color-coded neural tracts of tractography show the orientation of neural bundles equivalent to the body axes. A, anterior; D, dorsal; L, lateral. Scale bar: 1 mm. (A and B) Major neural bundles derived from the median basal lobe (mB) (horizontal section).
(C and D) Neural bundles associated within the peduncle lobe (Pe) (horizontal section).
(E and F) Neural bundles linked to the posterior pedal lobe (pP) and the ventral magnocellular lobe (vM) (horizontal section).
(G and H) Neural bundles in the dorsal basal lobe (dB) (sagittal section).

Based largely on the size and neuronal number within the squid brain (Young, 1974; Maddock and Young, 1987), we do not yet claim that what is presented here is a "brain atlas" or a "map" of the squid brain but just the beginning of one. As with vertebrate examples, using the complementary techniques of MRI, traditional histology, and dye-based tract tracing, this putative "circuit diagram" for squid neural architecture will lead to a better understanding of their complex behaviors. It also supports emerging hypotheses around anatomical and functional convergence with parts of the vertebrate CNS, including projections of overall body axes. Notably, it provides a firm base upon which to place the currently fashionable but contentious cephalopod cognitive capabilities. We hope that results here will encourage focal regions to be examined both for the new connections suggested and the actual functions they likely coordinate.

RESULTS

The Multi-lobed Squid Brain and Differentials of Lobe Growth Rate

Contrast-enhanced MR images (isotropic resolution 30 μm) of the brain of *S. lessoniana* allowed a re-examination of the known lobes of the squid brain and its three-dimensional (3D) detailed structure. Identification of brain lobes was based on the published anatomical studies as an initial aid in determining the boundaries between tissue types (Young, 1974, 1976, 1977, 1979; Messenger, 1979; Nixon and Young, 2003; Chung and Marshall, 2017) (Figures 1 and 2A). The 31 lobes (15 of which are bilateral) defined by Young's work (Young, 1974, 1976, 1977, 1979) on five similar loliginid species (Tables 1, S1, and S2) were identified here, but we suggest a further sub-division of the anterior chromatophore lobe into dorsal and ventral halves based on a clear within-lobe anatomical sub-division (Figures 1E, 8A, 8B, S1A–S1E, Tables 1, and S1). A series of MR image stacks (e.g., 11 slices for an olfactory lobe and 186 slices for an optic lobe of the smallest squid brain) allowed accurate volumetric estimates of the 47 lobes defined here, revealing distinct brain enlargement and corresponding morphological changes of lobes in the rapidly growing juvenile squid (n = 5) (Figures 1G, 1H, S1, and Table S1). Allometric analysis of the lobe complex volume showed significant variance of the slopes among 7 regression lines (ANOVA, df = 6, $p < 0.0001$). In particular, the palliovisceral lobe complex volume scales with positive allometry (slope 1.2645) and with a 95% confidence interval around the slope (1.1167–1.4124) excludes 1 (isometry). That is, this lobe complex grows disproportionately and its disproportionality increases with increased volume of the brain (Figure 1H).

dMRI and Tractography of the Squid Brain

Using HARDI, 30 diffusion-weighted orientations at a b-value of 3,000 s/mm^2 and two b0 images were acquired without diffusion weighting at the isotropic resolution 80 μm (n = 5) using a 16.4-T (700-MHz) vertical wide-bore micro-imaging system (Bruker Biospin, Karlsruhe, Germany) (detail in Methods). Validation of the squid tractography process was applied at multiple levels to quantify the match between the experimental estimated orientation and the true physical orientation of the fiber.

First, an initial comparison between full k-space (scan time approximately 39 h) and partial Fourier acceleration acquisitions (approximately 24 h) confirmed a high degree of similarity in defined fiber orientation distribution (FOD) in two squid specimens (Figures S3A and S3B). This includes, for example, the well-known optic nerves between optic lobes, four pairs of brachial nerves and funnel nerves (Figures S3A and S3B). As a result, with a realistic time frame in terms of scan and computation time in mind, another three specimens, so five in total, were scanned using this acceleration protocol (approximately 24 h for each individual) (Table S1). The following analyses were thus mainly based on data obtained using the accelerated protocol unless specifically noted.

Reconstructions of probabilistic tractography of the squid brain, where regions of interest (ROIs) and FOD are used, vary both in number and orientation with the selected algorithms and parameters chosen (see detail in Methods and Figures 2, 3, and 4). Cross-validation by spatially registering histological results and tractography was conducted, largely following protocols and caveats from previous HARDI brain

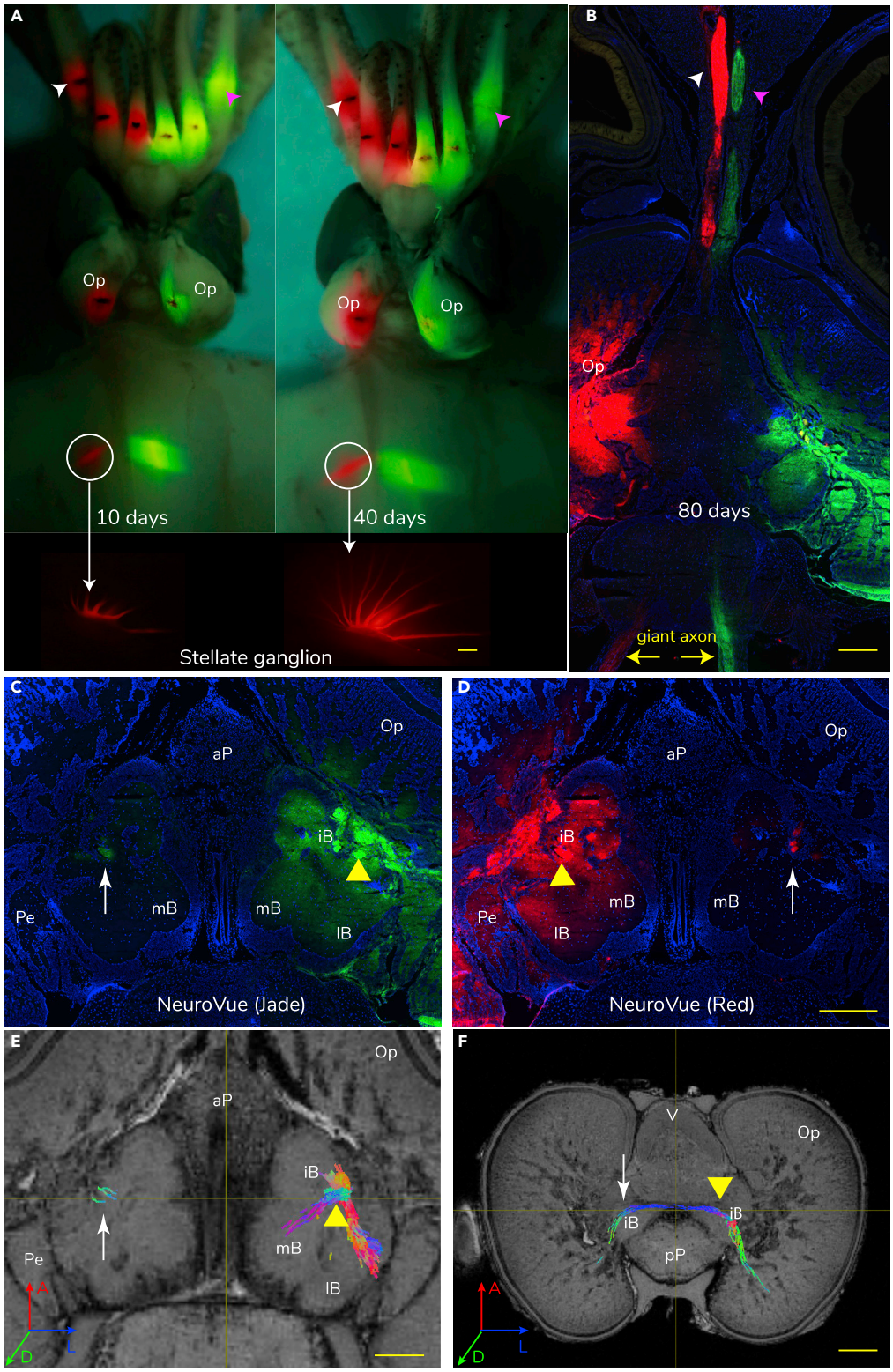

Figure 4. Lipophilic Dye Tracing of the Squid Neural Tracts

(A and B) An example of fluorescent dyes diffusion down squid neural tissue in a time series. (A) The lipophilic dye tracers, NeuroVue red (left) and jade (right), were applied symmetrically to parts of the squid neural tissue, including arms, optic lobes, and stellate ganglia. Arrows indicate the stellate ganglion; arrow heads indicate the dye diffusing along the

Figure 4. *Continued*

brachial nerve bundles. (B) A sample of slice showing that both dyes diffused along the brachial nerves of the third pair of arms with similar speed (arrow heads). Two yellow arrows indicate the stained giant axon, which the dyes were loaded into the stellate ganglion.

(C–E) Comparisons of the contralateral connection of the interbasal lobe (iB) tracts between the fluorescent dye tracing and tractography (horizontal section). (C and D) Triangles indicate that two dyes were loaded separately in the left and right iB, and arrows show the dye diffusion toward the contralateral side of iB. (E) Tractography projection of iB showing a good match to the dye tracing shown above.

(F) The same iB tractography was viewed in the transverse section. The color-coded neural tracts show the orientation of neural bundles equivalent to the body axes. A, anterior; D, dorsal; L, lateral. Scale bar: 1 mm.

studies (Valverde, 1998; Calamante et al., 2012; Kurniawan et al., 2014; Calabrese et al., 2015; Suarez et al., 2018). Two histological methods were used, the well-established method of Cajal-Golgi silver impregnation developed by Strausfeld (Strausfeld, 1980) with further modification (Figures 2B and 3) and a new lipophilic dye tracer NeuroVue (Shigeno et al., 2014) (Figures 2C, 2H, and 4) (see detail in Methods). After examining over 1,000 silver stains from 40 individuals, lipophilic dye tracing was then applied specifically to 42 targeted potential tracts to further clarify the silver staining results, particularly those with long contralateral connections that were often stained incompletely by silver impregnation, rendering 30 long tracts confirmed in five individual brains using multiple dye colors (Figures 2C, 2H, and 4B–4D).

Based on fiber geometries obtained from histology in this study and previous work by Young and Messenger (Young, 1974, 1976, 1977, 1979; Messenger, 1979; Nixon and Young, 2003), the selected lobes (e.g., basal, peduncle, and pedal lobes) were then used to test in detecting the choice of local fiber orientation and to optimize matches between tractography and histology (Figures 2, 3, 4, and S2). Imposing neuro-anatomical knowledge (e.g., trajectory of tracts of interest) to eliminate false positives led to increasingly accurate reconstruction of the local fiber architecture and lobe-to-lobe connectivity (Figures 2, 3, 4, 5, and S2). We then used the probabilistic algorithm and the optimized parameters defined by the 375 instances of exact anatomical match (silver-stained neurons or fluorescent tracing) to establish the lobe-dependent probabilistic tractography (Figures 5 and S2).

Squid whole-brain tractography results in an orientationally encoded color tract map, revealing an overall bilateral symmetry along any stereotaxis plane examined (Figures 3B, 3F, 4C–4F, 5A, S3, and S4 and Videos S2, S3, and S4). Using this color-coded map, the specific tracts of interest can be identified at a given slice level or three-dimensionally (Figures 2, 3, 4, 6, 7, 8, and S2). Specific tracts derived from lobes that are paired (Table 1 and Figures 2C, 2F–2H, 3A, 3B, 3E, 3F, 5, and S2) show network patterns precisely mirroring each other again providing confidence in their description as functional interconnections. Comparison between full k-space (long scan) and partial Fourier acceleration acquisitions confirmed a high degree of similarity for the squid whole-brain tractography (98.98% and 96.48% match in two individuals, respectively) (Figures S3C and S3D), suggesting no significant improvement for the mesoscale brain-wide tractography visualization and connectivity matrix under long scan and over-restrictive thresholding for tract acceptance (Figure S3). Probabilistic tractography data, pairwise connections, and the corresponding connectivity strength index (*Cs*: the logarithm of numbers of streamlines intersecting a pair of regions) were then used to generate a brain-wide neural connectivity matrix for each individual and the averaged connectivity matrix, respectively (Figures 5A, S3, and S4).

Among the 282 already known neural network pathways of squid brain described by Young and his colleague (Figure 5B) (Messenger, 1979; Young, 1974, 1976, 1977, 1979), the averaged connectivity matrix identified 281, that is, a 99.65% true-positive rate between previous Cajal-Golgi silver-stained results and tractography (range of *Cs* value: 0.477–5.084) (Figure 5A). This included 76 suggestions that were defined as possible tracts by Young (Young, 1974, 1976, 1977, 1979) (Figure 5B). The only one mismatch was the track between olfactory lobe and the lateral-ventral palliovisceral lobe (Figure 5B). In addition, 45 blank spots (*Cs* = 0) (Figure 5A) in the averaged connectivity matrix from tractography are well matched with the blanks from previous histology (Figure 5B).

Topographic Representation and Estimates of 145 New Interconnections

A mesoscale brain-wide tractography-based connectivity matrix for squid with an additional 145 (*Cs* > 2.7) previously unknown lobe-lobe tracts is proposed here (Figure 5C). Ninety-three new tracts (64.14%) were

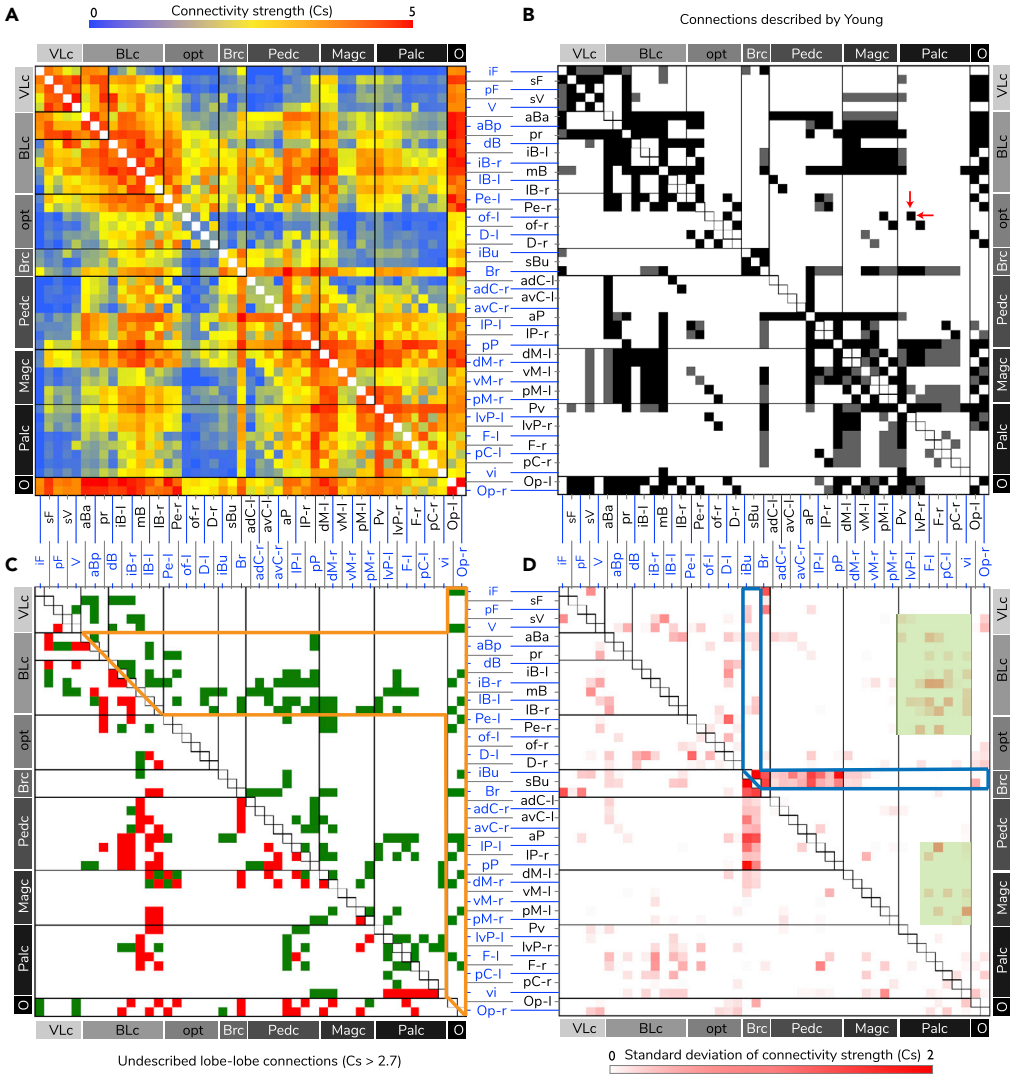

Figure 5. Connectivity Matrices of the Squid Brain

(A) An averaged probabilistic tractography connectivity matrix of five individuals. The heatmap indicates $\log_{10}$-transfered connection strength (*Cs*).

(B) This matrix summarized all described lobe-lobe neural connections of the loliginid squid, including 282 neural connections based on the Cajal-Golgi impregnation results by J.Z. Young and his colleagues (Young, 1974, 1976; 1977, 1979; Messenger, 1979). Black squares indicate the well-defined tracts; gray squares are the partially stained ones that were defined as possible tracts by Young. Red arrows indicate the only tract (between olfactory lobe and the lateral-ventral palliovisceral lobe) that was not recovered from the averaged tractography matrix.

(C) The new lobe-to-lobe tracts and their distribution pattern. This matrix is visualized against the known 282 tracts and is subtracted from all tracts recovered by the selected conservative *Cs* of 2.7, suggesting 145 new tracts (green squares) where 93 have been confirmed by histology (red squares). The highlighted region (within the orange line) contains over 62% of these new tracts for which the tractographic connection patterns are likely to response to the visual-motor control.

(D) Matrix summarizing the pairwise connections (red squares) with a high degree of variation of *Cs* among the five individuals. The region within the blue line shows high variation of *Cs* due to two damaged buccal lobes in two samples (see Figure S1B and Table S1) during brain extraction and a resulting low connection strength. The green shaded areas contain regions showing rapid lobe enlargement (lower motor control-related lobes) inducing increased values of *Cs*. See also Figures S1, S3, and S4; Table S1; Videos S2, S3, S4, and S5.

also confirmed with Cajal-Golgi or dye tracing (Figure 5C). We are confident in the remaining 36%, currently without direct backup from Cajal-Golgi or dye tracing, owing to both the highly conservative methods just described and the great match rate between previous connections identified and our results.

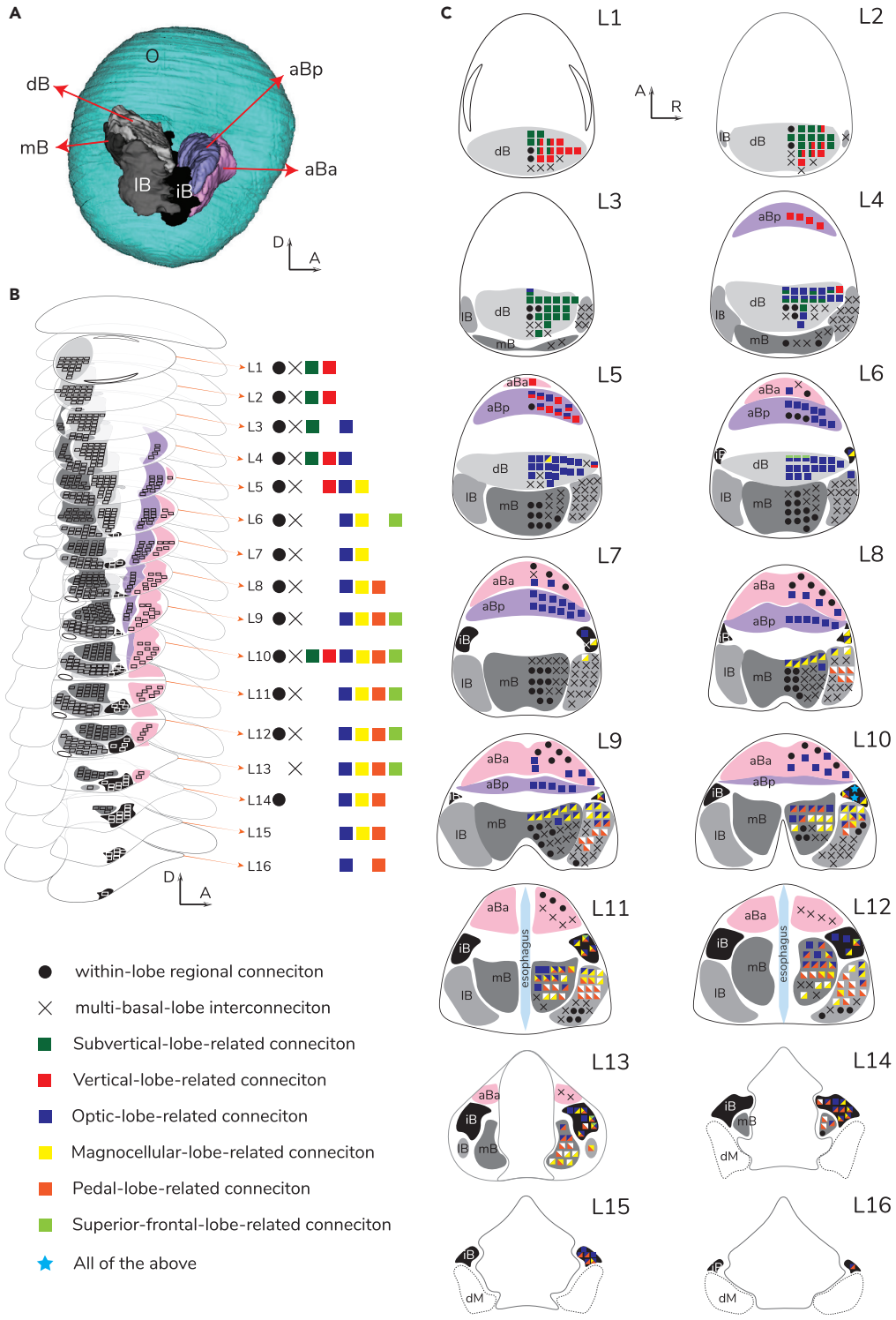

Figure 6. The Neural Network of the Multi-layered Basal Lobe System

(A) 3D reconstruction of the basal-optic lobe system. D, dorsal; A, anterior; R, right side of animal. Other abbreviations as in Table 1.

(B) Schematic drawings represented the subdivided small regions of interest (ROIs color and symbol coded as in Key) (n = 604) in the right half of the basal lobe system throughout the dorsoventral axis (16 levels L1–L16, each level thickness is 120 μm).

Figure 6. *Continued*

(C) Schematic drawings represented the dominant connectivity patterns between the ROIs and the projection lobe(s) throughout this system. Along with tractography derived from these small ROIs, the dominant connectivity of each ROI is identified by the color-coded symbols, revealing the detailed tractographic network of this high-order visual-motor control center. Two blue stars in the interbasal lobe at level 10 indicate that all eight types of connections can be found in these two ROIs.

See also Video S5.

Over 62% of the 145 new structural connections are linked to the vision (optic lobes) and motor control (basal lobes) systems (Figure 5C). Sixty-seven of these are found within the basal lobe system, a brain area controlling higher motor activity, and another 23 tracts connecting the optic lobes to other brain areas (Figures 5C, 6, 7, and 8). The already well-known chiasma of optic nerves and the associated projections toward the outer granule layer of the optic lobe can be clearly identified (Videos S3 and S5). As the secondary visual nerves enter the medulla of the optic lobe, tractography presents a previously unseen grid-like network of ongoing connections (Figure 7 and Video S5). The peripheral retinotopicity that optic chiasma allows (Figure 7 and Video S5) apparently travels deeper within the optic lobe than previously noted (beyond the zone of radial columns described by Young [1974]) and this most likely impacts processing of visual information. Interestingly, at this point in the optic lobe medullary region, there are many motor control circuits that directly couple to this network and project to the basal lobe (Figures 6 and 7 and Video S5). This would allow a topographical overlay of the outside world as viewed by the eye on the motor command units controlling locomotion (fins and funnel) and use of arms as discussed later (Figure 6). This provides another example of convergence with the vertebrate brain as noted by Shigeno et al. (2018) before the strong supporting evidence that we provide here.

The tracts of the basal lobe system divide into two major orientations, one ipsilateral and one contralateral as shown in the neural connectivity matrix (Figures 2F–2H, 3A, 3B, 4C–4F, 5, and 7). The contralateral tracts include those going from the left anterior-median lobule of the anterior basal lobe (aBa) to the right optic lobe and some that travel from the right anterior-median lobule of the aBa to the left optic lobe (Figures 2F–2H). There are also two separate contralateral connections between the left and right interbasal lobes joining the left and right lateral basal lobes, for example (Figure 5A). Aside from examining the lobe-dependent tractography, with the distinct anatomical features of the neighbor basal lobes, examination of the basal lobe system of the smallest brain by dividing its right half into 604 small ROIs (each ROI voxel = 120 μm × 120 μm × 120 μm) evenly distributed across this system throughout the dorsoventral axis revealed that the corresponding tractography of ROIs represents specified neural connectivity patterns distributing in 16 levels (L1–L16) (Figure 6). The spatial arrangement here is complex but highly organized containing elements of the visual and lower motor control areas (Figures 6 and 7). Overall, the basal lobes construct a well-defined relay station. For example, in the upper region of the basal lobe system, there are interconnections between the vision (optic lobes) and the memory formation and learning areas (vertical and subvertical lobes). There is also a complex set of serially interconnected networks at different depth levels allowing signal-relay wiring patterns between vision (optic lobes) and lower motor centers (e.g., pedal and magnocellular lobes), mediating with eye movement, locomotion by funnel and fins. More specifically these networks identified include:

(1) The upper levels of the dorsal basal lobe (L1 and L2) and anterior basal lobes (L4 and L5) show direct connection with the learning and memory center, including vertical and subvertical lobes (Figures 5 and 6). The power of HARDI is evident here as previous work missed the connections between the basal lobe and the vertical lobe entirely (Young, 1977).

(2) There are a significant number of short tracts forming a complex network within adjacent basal lobe regions (e.g., dorsal, median, and lateral basal lobes throughout the basal lobe system, Figure 6).

(3) A multilayered structure found in all basal lobes could retain the spatial information projecting from the optic lobe. Projections from the upper layers of the basal lobes connect only with the upper level of the optic lobe, whereas the projections from the lower levels of the basal lobes shift toward lower levels of the optic lobe accordingly (Figure 7 and Video S5). This forms an orderly topographical representation from the basal lobe system toward the medulla of the optic lobe at different depth levels (L3–L16) (Figures 6 and 7).

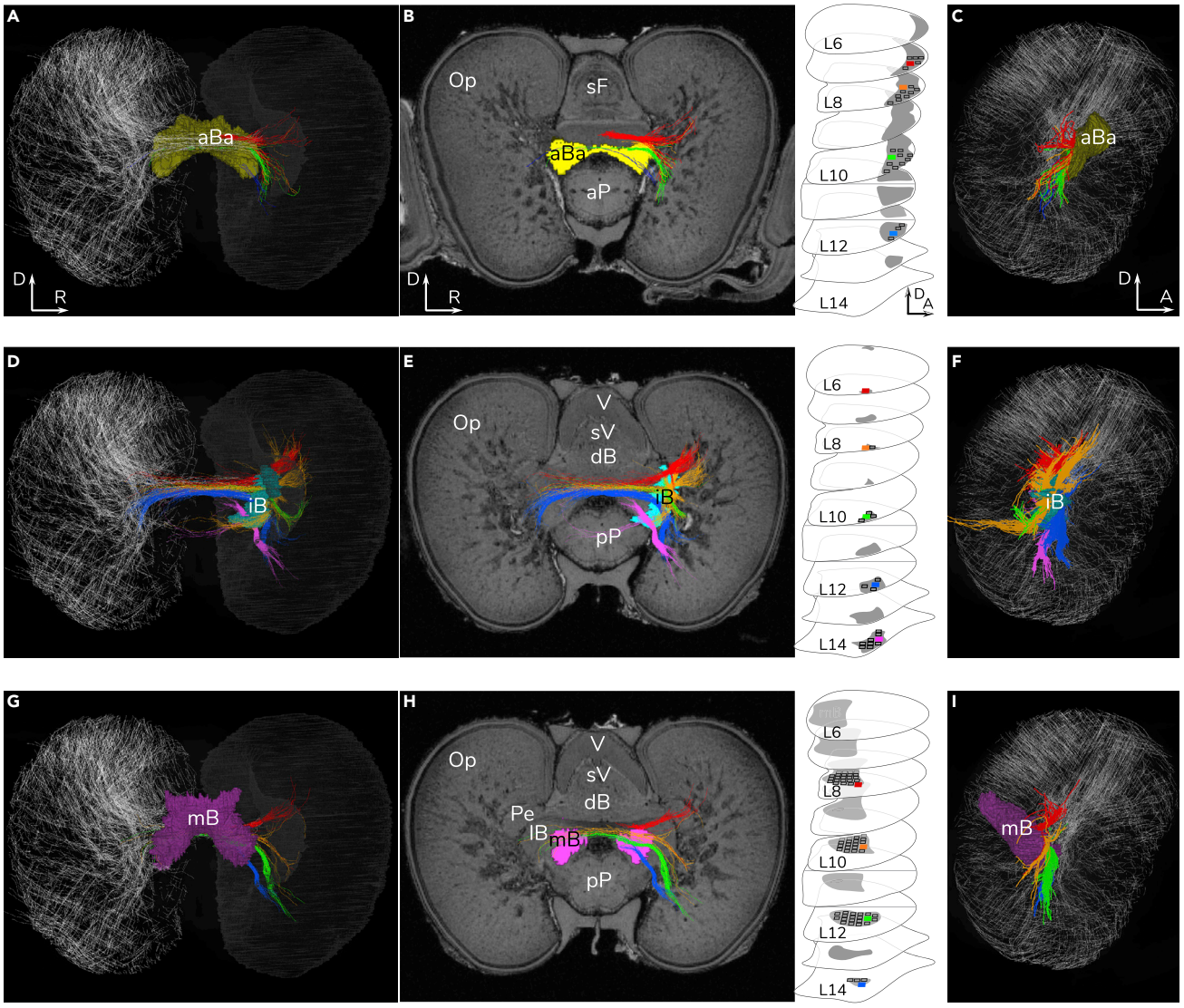

Figure 7. Topographic Representation in the Optic Lobe and Basal Lobe Connections

(A–C) Anterior basal lobe (aBa). D, dorsal; A, anterior; R, right side of animal. (A) 3D reconstruction of this optic-basal system. To visualize the grid-like network in the medulla of the left optic lobe, 0.5% of the streamlines extracted from the probabilistic tractography of the optic lobe were used here. This structural network may function to keep the peripheral retinotopicity deeper within the medulla of optic lobe and directly couple to the tracts of aBa. (B) Transverse section showing the color-coded aBa tracts of level 7 (red), 8 (orange), 10 (green), and 12 (blue) and the levels of the basal lobe system (the same as Figure 4) shown to the right. The corresponding projections ended in different layers of the medulla (dorsoventral plane). (C) The distribution of the aBa projections inside the medulla viewed from the side. Detailed 3D geometric information of projections can be found in Video S5.

(D–F) Interbasal lobe (iB). (D) 3D reconstruction of the optic-interbasal system and the associating tracts. (E) Transverse section showing the color-coded tracts of level 6 (red), 8 (orange), 10 (green), 12 (blue), and 14 (pink). (F) The distribution of the iB projections inside the medulla.

(G–I) Median basal lobe (mB). (G) 3D reconstruction of the optic-median basal system and the associating tracts. (H) Transverse section showing the color-coded tracts of level 8 (red), 10 (orange), 12 (green), and 14 (blue). (I) The distribution of the mB projections inside the medulla.

See also Video S5.

(4) The median-basal layers (L5–L16) mediate lower motor control including connections to arm movements (pedal lobes) and funnel and fin movements (magnocellular lobes). Most of these motor control tracts are congruent with optic relay pathways, suggesting a role in visual-motor coordination (Figures 5, 6, and 7).

(5) New interconnections in response to coloration control are described where the dorsal area of the anterior chromatophore lobe projects mainly to the head and the ventral area to the arms (Figures

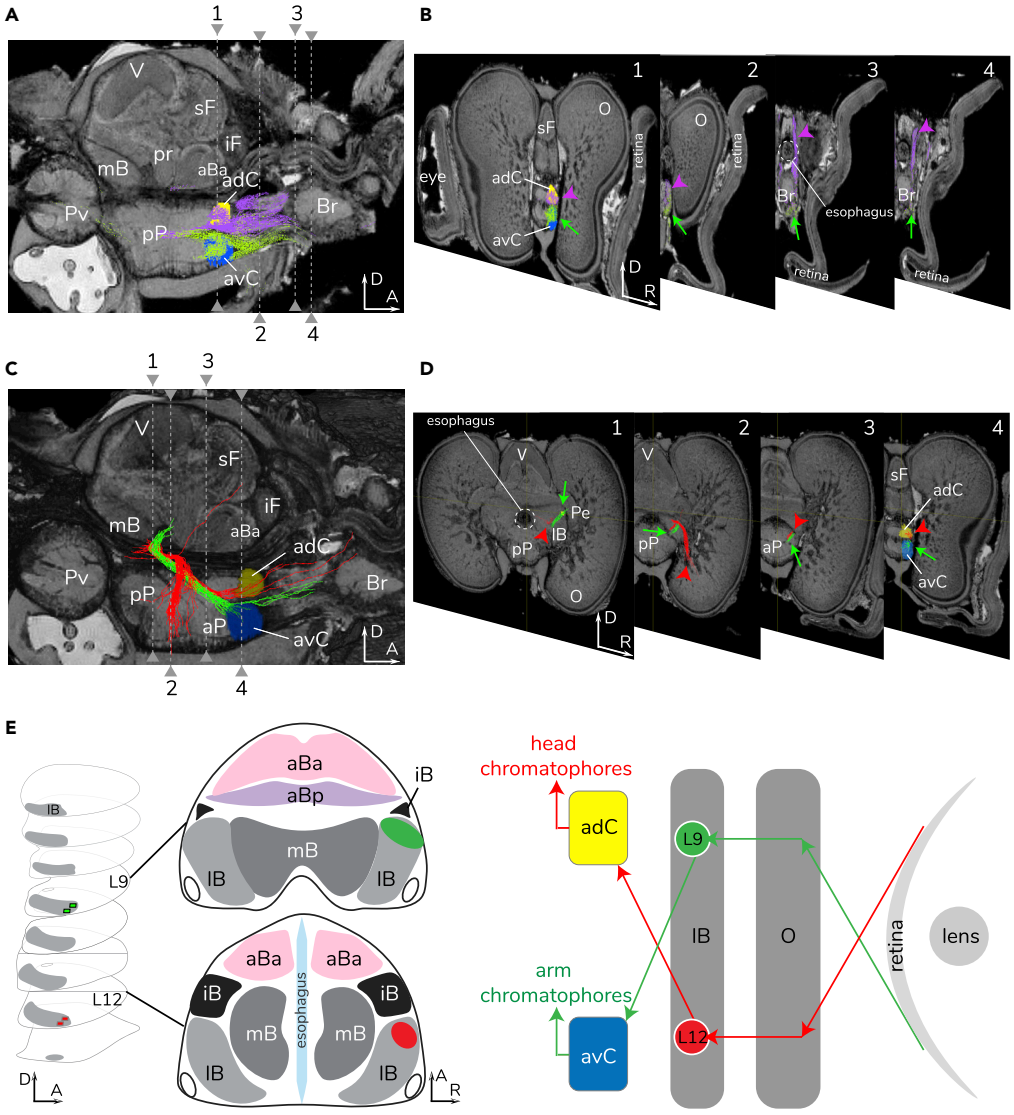

Figure 8. A Second Chiasm in the Coloration Control Circuit

(A) Two color-coded tracts derived from the two anterior chromatophore lobes, including the purple tracts of the anterior dorsal chromatophore lobe (adC) and the green tracts of the anterior ventral chromatophore lobe (avC). D, dorsal; A, anterior; R, right side of animal.

(B) Four transverse sections (from posterior to anterior) showing the progression of the purple tracts of adC toward the head (arrow heads) and the green tracts of avC toward arms (green arrows).

(C) Two additional circuits proposed here from Levels 9 and 12 of the basal lobe system (see Figure 4, and color-coded green and red, respectively, throughout the figure) linking adC and avC to the lateral basal (IB) and optic (O) lobes (sagittal section), forming a second chiasm.

(D) Four transverse sections (from posterior to anterior) showing the progression of green and red tracts toward the avC (green arrows) and the adC (red arrow heads).

(E) A schematic drawing of this second chiasm and the levels of the lateral basal lobe shown to the left.

8A and 8B). Furthermore, two additional circuits linked to the anterior chromatophore lobes and the resulting second chiasm are identified: (i) the lateral basal lobe (L9) to the anterior ventral chromatophore lobe and (ii) the lateral basal lobe (L12) to the anterior dorsal chromatophore lobe control arm and head chromatophores, respectively (Figures 8C–8E). This second chiasm forms a previously unknown dorsoventral cross-over between the optic lobe and the chromatophore lobes via the basal lobe system (Figures 8C–8E).

(6) A unique connection has been found between the dorsal basal and superior frontal lobe at L6, derived from the interbasal lobe at different depth levels (L9–13). The potential function of this connection is unknown in squid (Figure 6). In octopus the superior frontal lobe is involved in chemosensory learning and memory (Boycott, 1965; Wells, 1963).

DISCUSSION

Using the modern imaging techniques of high-resolution dMRI that we adapted from established vertebrate methods combined with both old (Golgi) and new (NeuroVue) histological results, we have started the first mesoscale MRI-based cephalopod brain atlas. New insights reveal inter-individual variability of squid brain in both volumetric and tractographic network aspects. This dataset provides a foundation for proposing new functional morphology and interactions between brain regions. It also supports emerging hypotheses around anatomical and functional convergence with parts of the vertebrate central nervous system (Packard, 1972; Shigeno et al., 2018).

New Pathways and Functional Importance

Squid are voracious predators using their "simple eyes" to conduct a vision-dominated lifestyle. Their eye is famously convergent to the vertebrate eye (Packard, 1972; Chung and Marshall, 2017; Hanlon and Messenger, 2018), but although much is known about the optical and retinal elements (Sweeney et al., 2007; Chung and Marshall, 2014, 2016, 2017; Gagnon et al., 2016), the optic lobe remains one of the most mysterious neural integration centers in visual neuroscience (Cajal, 1917; Boycott, 1961; Young, 1974; Liu and Chiao, 2017; Liu et al., 2018). The pioneering neuroanatomical work of Cajal (cuttlefish and squid) and Young (octopus and squid) demonstrated a retinal topography preserved through to the retina profunda, the outer layers of the optic lobe (Cajal, 1917; Young, 1971, 1974). Also known as deep retina, this is where neurons of the outer and inner granular layers are assumed to process visual input and retinotopicity was known to remain (Young, 1974). That is, a general plan of the outside world remained fixed to the two-dimensional layout of the layers present. Before our work here, deeper into the optic lobe, the amorphous arrangement of the millions of neurons within the medulla made anatomical or functional correlations difficult. The tractography presented here now demonstrates a clear grid-like and retinotopic network that is maintained deep within the medulla of the optic lobes and indeed well beyond it to other brain areas (Figure 7 and Video S5). This network of cells was described by Young as centrifugal axons, multipolar cells, large horizontal cells, and efferent neurons connected with other lobes, and with a *possible organization* that we now confirm (Young, 1974) (Figure 7 and Video S5). Based on tractography of the optic lobe, this grid structure initially appears below the inner granular layer and is continuous within the medulla, forming a layered organization. Although the projections of the basal lobes into the medulla apparently reach different locations and depths (Figure 7 and Video S5), neural coding via spatial and temporal coherence via this grid network could integrate visual signals and coordinate complex vision-related activities. If that is the case, there are parallels to similar mechanism in vertebrate's visual cortex (Hubel and Wiesel, 1968; Shigeno et al., 2018). This structure-function link now makes it possible to support the idea of a retinal topographic representation connected through to two previously known somatotopic maps, including the anterior-median lobule of the aBa (control of posture and movement of head and eyes) (Young, 1977) and the peduncle lobe (coordinating motor activities) (Messenger, 1979). In addition, our new tractography adds two further topographic representations in the basal lobe system, specifically in the median and inter basal lobes (Figures 6 and 7 and Video S5). This again underlines the orderly topographic congruence of visual scene and motor control system that Young originally proposed but lacked evidence for (Young, 1974, 1977). Counter suggestions since Young in fact suggested that a somatosensory congruence in cephalopods was unlikely (Zullo et al., 2009; Liu and Chiao, 2017).

Shigeno et al. (2018) recently highlighted similarities between cephalopod and vertebrate brains in terms of lobe organization, functional analogies, and development. They equated, for example, the optic lobe to the vertebrate tectum, dorsal basal lobe to thalamus, and anterior basal lobe to basal ganglia. This again follows the original suggestions of convergence of the cephalopod and vertebrate brain from Young (1971) and adds to a growing body of literature finding parallels between vertebrate and invertebrate brains and their functional sub-units (Packard, 1972; Shigeno et al., 2018). There are well-known and orderly topographic maps of a variety of sorts with both sensory and somatic origins in vertebrate cortex (Penfield and Boldrey, 1937; Kaas, 1997; Jbabdi et al., 2013). The squid tractography we present here suggests another example of convergence in visual systems, adding to that of the more famous optical arrangement of the eye and the initial suggestions from Boycott (1961) and Young (1974). We hope that the detail and

new features of this outside map to spatio-motor control will guide research in function, behavior, and cognition.

Another new feature of squid brain that our combined MRI/dye-trace/histology approach can map is the highly subdivided network of the basal lobe system (Figure 6). As noted in the vertebrate cortex (Hubel and Wiesel, 1962; Alexander et al., 1986), within-lobe and inter-lobe connections at different levels may group neurons that frequently interact and provide a processing platform with short interconnections. These sorts of functional groupings overcome some of the distributed network problems in brain design (Kaas, 1997; Betzel and Bassett, 2017; Lynn and Bassett, 2019), a solution noted in *Drosophila* and *Caenorhabditis* connectomics also (White et al., 1986; Shih et al., 2015; Cook et al., 2019). We suggest that the multi-layered basal lobe system, which receives visual scene input from the optic lobe (Figures 6 and 7) may translate and distribute the control commands in a spatiotemporal manner to different motor units. These include direction of tentacular strike, schooling, arm coordination over the outside visual field, and courtship display through body posture and color changes (Jantzen and Havenhand, 2003; Mather et al., 2010; Sugimoto and Ikeda, 2012; Lin et al., 2017; Hanlon and Messenger, 2018). This latter possibility deserves further elaboration using electrical recording, stimulation, and biochemical studies.

Multiple Levels of Control in Coloration and Patterns

The rapidity and versatility of body color and pattern change in cephalopods for both communication and camouflage is almost legendary (Jantzen and Havenhand, 2003; Mather et al., 2010; How et al., 2017; Lin et al., 2017; Hanlon and Messenger, 2018; Reiter et al., 2018). The skin elements, chromatophores, iridophores, and leucophores, are under direct neural control in response to visual perception of environment as well as behavioral mood changes (Darmaillacq et al., 2014; How et al., 2017; Hanlon and Messenger, 2018). Using computational analysis to quantify the states of chromatophores of live cuttlefish revealed that a hierarchical motor control mechanism governs development of skin patterns and dynamic coloration (Laan et al., 2014; Reiter et al., 2018). This view is also supported by both neuroanatomical, electrophysiological, and now our tractography approaches, suggesting that this skin-display system is hierarchically organized via the optic, lateral basal, peduncle, and chromatophore lobes (Boycott, 1961; Young, 1974; Dubas et al., 1986; Novicki et al., 1990) (Figures 6 and 8).

Our tractography and mapping also provides new evidence for a sub-division of the anterior chromatophore lobe into dorsal and ventral units in squid, the dorsal lobe controlling dorsal head color and ventral, arm color (Figures 8A and 8B). The two paired anterior chromatophore lobes may link body form and color display while squid hover in water column such as countershading camouflage that a task is distinct to the benthic octopus, which retains only one pair of anterior chromatophore lobes (Young, 1971). The reason for this is explored next.

A new chiasm is clear from the tractography presented here, between the lateral basal lobe and the anterior chromatophore lobes (Figures 8C–8E). This second dorsoventral crossing of tracts within the coloration control circuit we hypothesize may control open water countershading camouflage. The second chiasm ensures the seafloor image falling on the dorsal retina is sent to the anterior dorsal chromatophore lobe, which controls dark coloration on the head to match with the seafloor background. The other tract would guide the ventral side of head and arms to show light color patterns to match with the visual scene above the squid. Aside from this proposed coloration circuit, a similar chiasm-like network for the coordination of head and eye movement was previously noted in the anterior-median lobule of the aBa by Young (1977) (confirmed here also by our tractography and dye tracing [Figures 2F–2H]). This kind of crossing arrangement could be a common feature of the basal lobe system (Young, 1977). Chiasmata in any nervous system are of interest owing to mapping inversions and other non-linear relationships as well as re-configuration of evolutionary trajectory of vision and visual behaviors (Sinakevitch et al., 2003; Strausfeld, 2005).

A Comparison between Cephalopod Species

Table S2 lists the loliginid squid species including the five species from the North Atlantic Ocean (Young, 1974, 1976, 1977, 1979; Messenger, 1979; Wild et al., 2015) and *S. lessoniana* from the Indo-Pacific Ocean (Shigeno et al., 2001; Kobayashi et al., 2013), our work here, upon which much of our knowledge of the squid brain is based. Despite different geographic distribution and phylogenetic differences (six species from three genera where the genus *Sepioteuthis* is the stable basal in-group taxa in family Loliginidae) (Anderson, 2000; Strugnell et al., 2005; Vecchione et al., 1998), organization of the CNS, number of lobes in the

circum-esophageal ring, and the interregional connections are very similar between species. Perhaps more surprising, a comparison between cuttlefish and squid also indicates these coleoid groups (decapodiform) share a basically similar layout (Cajal, 1917; Boycott, 1961; Young, 1974, 1976, 1977, 1979; Messenger, 1979; Nixon and Young, 2003). The decapodiform cephalopods may mirror brain organization bauplans from the life needs of a rapid visual predator and also conduct courtship display in the water column.

Considering the evolutionary divergence time of major cephalopod groups (Strugnell et al., 2006), the brain maps of cuttlefish, octopus, and vampire squid using the techniques developed here are underway. In contrast to the elongated CNS arrangement in decapodiforms, the compact octopus brain (octopodiform) has evolved distinct changes, particularly the noticeable five gyri of the vertical lobe (learning and memory) and sub-divisions of the frontal lobe system (tactile and chemosensory) (Wells, 1963; Boycott, 1965; Young, 1971; Shigeno and Ragsdale, 2015). Development of these octopus-specialized lobes is likely linked to their benthic life such as searching invisible food from crevices using nimble arms. Furthermore, the vampire squid (the basal clade of coleoids), which inhabits in midwater (ca. 600–1,000 m depth), possesses features of both octopodiform and decapodiform in body form (e.g., eight arms with two tentacle-like filaments) and brain organization (squid-like suboesophageal and octopus-like supraoesophageal mass) (Young, 1964; Nixon and Young, 2003). A comparison between coleoid brains could further extend our understanding of the evolutionary history between cephalopod brain design and life styles.

We erect the start of a connectome for the squid brain, the first of its kind for the cephalopods with input from high-resolution dMRI, previous histology, new histology with old (Cajal-Golgi silver impregnation), and new fluorescent neuronal tracers. This study does not claim to build a complete connectivity atlas but to erect an initial predictive mesoscale connectome that reveals hitherto unsuspected pathways. As is the result of any connectome, several new functional circuits are suggested by this map, as well bolstering the previously known functional sub-units that underlie behaviors. The apparently complex cognitive tasks cephalopods perform need this kind of solid background evidence before anthropomorphic speculations lead to misconceptions around these unique and wonderful creatures.

Limitations of the Study

This study reveals the first mesoscale MRI-based neural connectivity in the squid brain; however, it is possible that some limitations could affect the results presented here.

Indirect Quantitative Measurement of Tractography: Visualization of 3D direction-coded color tractography of the squid brain reveals rich information that is not possible to see in conventional histology. However, the MRI-based tractography is based on a mapping from water diffusion to fiber orientation. In other words, an estimate of the confidence on the route of least hindrance to diffusion can thus indirectly reflect the connecting neural bundles between pairs of regions, making analysis of tractography and the resulting connectivity matrix less quantitative. Detailed advantages and potential pitfalls about the tractography can be found in the review by Sotiropoulos and Zalesky (2019).

Species Selection: Our current knowledge of the neural network of the squid brain is majorly based on a series of studies in the nervous system of *Loligo* (Young, 1974, 1976, 1977, 1979; Messenger, 1979). It is worth noting that the five species (see Table S2) used in Young's studies are phylogenetically close to the species used in this study. Some new findings in this study (i.e., subdivisions of lobes and new tracts) might be arguable owing to species selection. Although all five species in Young's study are not available in Australian waters, selecting *S. lessoniana* is a good start and a reliable bridge to the classical studies of loliginid squid.

No Information of Synaptic Connection: Our current macroscale tractography and histological results are unable to reveal synaptic connections yet. Further efforts to label neural tracts and comparative studies across different cephalopod groups are ongoing, and hopefully will lead to further defined neural connectivity in cellular level.

METHODS

All methods can be found in the accompanying Transparent Methods supplemental file.

DATA AND CODE AVAILABILITY

The authors confirm that the data supporting the findings of this study are available within the article, its Supplemental Information, and Mendeley Data (https://doi.org/10.17632/pwkh3s2t33.1).

SUPPLEMENTAL INFORMATION

Supplemental Information can be found online at https://doi.org/10.1016/j.isci.2019.100816.

ACKNOWLEDGMENTS

This work is supported by the Australian Research Council (ARC) (FL140100197) (Australian Laureate Fellowship to N.J.M.). The 16.4 T is supported by the Queensland State Government through the Queensland NMR Network and the Australian Government through National Collaborative Research Infrastructure Strategy (NCRIS) and the National Imaging Facility. Histological imaging was performed at the Queensland Brain Institute's Advanced Microscopy Facility using Zeiss Axio Imager.

AUTHOR CONTRIBUTIONS

W.-S.C designed and performed most experiments and analysis and wrote the first version of the manuscript. N.D.K. and W.-S.C. performed MRI and tractography. N.J.M. supervised the project and co-wrote the manuscript with input from all authors. All authors contributed to data analysis, interpretation, and revision of the manuscript.

DECLARATION OF INTERESTS

The authors declare no competing interests.

Received: August 14, 2019
Revised: December 11, 2019
Accepted: December 27, 2019
Published: January 24, 2020

REFERENCES

Abbott, N.J., Williamson, R., and Maddock, L. (1995). Cephalopod Neurobiology (Oxford University Press).

Albertin, C.B., Simakov, O., Mitros, T., Wang, Z.Y., Pungor, J.R., Edsinger-Gonzales, E., Brenner, S., Ragsdale, C.W., and Rokhsar, D.S. (2015). The octopus genome and the evolution of cephalopod neural and morphological novelties. Nature *524*, 220–224.

Alexander, G.E., Delong, M.R., and Strick, P.L. (1986). Parallel organization of functionally segregated circuits linking basal ganglia and cortex. Annu. Rev. Neurosci. *9*, 357–381.

Alomair, O.I., Brereton, I.M., Smith, M.T., Galloway, G.J., and Kurniawan, N.D. (2015). In vivo high angular resolution diffusion-weighted imaging of mouse brain at 16.4 Tesla. PLoS One *10*, e0130133.

Anderson, F.E. (2000). Phylogeny and historical biogeography of the loliginid squids (Mollusca: cephalopoda) based on mitochondrial DNA sequence data. Mol. Phylogenet. Evol. *15*, 191–214.

Assaf, Y., Johansen-Berg, H., and Thiebaut de Schotten, M. (2019). The role of diffusion MRI in neuroscience. NMR Biomed. *32*, e3762.

Aydogan, D.B., Jacobs, R., Dulawa, S., Thompson, S.L., Francois, M.C., Toga, A.W., Dong, H.-W., Knowles, J.A., and Shi, Y.-G. (2018). When tractography meets tracer injections: a systematic study of trends and variation sources of diffusion-based connectivity. Brain Struct. Funct. *223*, 2841–2858.

Bassett, D.S., and Sporns, O. (2017). Network neuroscience. Nat. Neurosci. *20*, 353–364.

Betzel, R.F., and Bassett, D.S. (2017). Multi-scale brain networks. Neuroimage *160*, 73–83.

Boycott, B.B. (1961). The functional organization of the brain of the cuttlefish *Sepia officinalis*. Proc. Biol. Sci. *153*, 503–534.

Boycott, B.B. (1965). Learning in the Octopus. Sci. Am. *212*, 42–50.

Boycott, B.B., and Young, J.Z. (1955). A memory system in *Octopus vulgaris* Lamarck. Proc. Biol. Sci. *143*, 449–480.

Boycott, B.B., and Young, J.Z. (1957). Effects of interference with the vertical lobe on visual discriminations in *Octopus vulgaris* Lamarck. Proc. Biol. Sci. *146*, 439–459.

Brown, E.R., Piscopo, S., de Stefano, R., and Giuditta, A. (2006). Brain and behavioural evidence for rest-activity cycles in *Octopus vulgaris*. Behav. Brain Res. *172*, 355–359.

Bublitz, A., Weinhold, S.R., Strobel, S., Dehnhardt, G., and Hanke, F.D. (2017). Reconsideration of serial visual reversal learning in octopus (*Octopus vulgaris*) from a methodological perspective. Front. Physiol. *8*, 54.

Bullmore, E., and Sporns, O. (2009). Complex brain networks: graph theoretical analysis of structural and functional systems. Nat. Rev. Neurosci. *10*, 186–198.

Bullock, T.H., and Horridge, G.A. (1965). Structure and Function in the Nervous Systems of Invertebrates (Freeman).

Cajal, S.R. (1917). Contribucion al conocimiento de la retina y centros opticos de los cefalopodos. Tarbajos del laboratorio de investigacious biologicas de la universidad de Madrid *15*, 1–82. https://bipadi.ub.edu/digital/collection/atlesmed/id/103317.

Calabrese, E., Badea, A., Cofer, G., Qi, Y., and Johnson, G.A. (2015). A diffusion MRI tractography connectome of the mouse brain and comparison with neuronal tracer data. Cereb. Cortex *25*, 4628–4637.

Calamante, F., Tournier, J.D., Kurniawan, N.D., Yang, Z., Gyengesi, E., Galloway, G.J., Reutens, D.C., and Connelly, A. (2012). Super-resolution track-density imaging studies of mouse brain: comparison to histology. Neuroimage *59*, 286–296.

Chrachri, A., and Williamson, R. (1998). Synaptic interactions between crista hair cells in the

statocyst of the squid *Alloteuthis subulata*. J. Neurophysiol. *80*, 656–666.

Chung, W.-S., and Marshall, N.J. (2014). Range-finding in squid using retinal deformation and image blur. Curr. Biol. *24*, R64–R65.

Chung, W.-S., and Marshall, N.J. (2016). Comparative visual ecology of cephalopods from different habitats. Proc. Biol. Sci. *283*, 20161346.

Chung, W.-S., and Marshall, N.J. (2017). Complex visual adaptations in squid for specific tasks in different environments. Front. Physiol. *8*, 105.

Cook, S.J., Jarrell, T.A., Brittin, C.A., Wang, Y., Bloniarz, A.E., Yakovlev, M.A., Nguyen, K.C.Q., Tang, L.T., Bayer, E.A., Duerr, J.S., et al. (2019). Whole-animal connectomes of both *Caenorhabditis elegans* sexes. Nature *571*, 63–71.

Darmaillacq, A.-S., Dickel, L., and Mather, J.A. (2014). Cephalopod Cognition (Cambridge University Press).

Deweerdt, S. (2019). Deep connections. Nature *571*, S6–S8.

Donahue, C.J., Sotiropoulos, S.N., Jbabdi, S., Hernandez-Fernandez, M., Behrens, T.E., Dyrby, T.B., Coalson, T., Kennedy, H., Knoblauch, K., van Essen, et al.. (2016). Using diffusion tractography to predict cortical connection strength and distance: a quantitative comparison with tracers in the monkey. J. Neurosci. *36*, 6758–6770.

Dubas, F., Hanlon, R.T., Ferguson, G.P., and Pinsker, H.M. (1986). Localization and stimulation of chromatophore motoneurons in the brain of the squid, *Lolliguncula brevis*. J. Exp. Biol. *121*, 1–25.

Edsinger, E., and Dölen, G. (2018). A conserved role for serotonergic neurotransmission in mediating social behavior in octopus. Curr. Biol. *28*, 3136–3142.

Fiorito, G., and Scotto, P. (1992). Observational learning in *Octopus vulgaris*. Science *256*, 545–547.

Gagnon, Y.L., Osorio, D.C., Wardill, T.J., Marshall, N.J., Chung, W.-S., and Temple, S.E. (2016). Can chromatic aberration enable color vision in natural environments? Proc. Natl. Acad. Sci. U S A *113*, E6908–E6909.

Grasso, F.W. (2014). The octopus with two brains: how are distributed and central representations integrated in the octopus central nervous system? In Cephalopod Cognition, A.-S. Darmaillacq, J. Mather, and L. Dickel, eds. (Cambridge University Press), pp. 94–122.

Hanlon, R.T., and Messenger, J.B. (2018). Cephalopod Behaviour (Cambridge University Press).

How, M.J., Norman, M.D., Finn, J., Chung, W.-S., and Marshall, N.J. (2017). Dynamic skin patterns in cephalopods. Front. Physiol. *8*, 393.

Hu, M.Y., Yan, H.Y., Chung, W.-S., Shiao, J.C., and Hwang, P.P. (2009). Acoustically evoked potentials in two cephalopods inferred using the auditory brainstem response (ABR) approach. Comp. Biochem. Physiol. A Mol. Integr. Physiol. *153*, 278–283.

Hubel, D.H., and Wiesel, T.N. (1962). Receptive fields, binocular interaction and functional architecture in the cat's visual cortex. J. Physiol. *160*, 106–154.

Hubel, D.H., and Wiesel, T.N. (1968). Receptive fields and functional architecture of monkey striate cortex. J. Physiol. *195*, 215–243.

Jantzen, T.M., and Havenhand, J.N. (2003). Reproductive behavior in the squid *Sepioteuthis australis* from south Australia: ethogram of reproductive body patterns. Biol. Bull. *204*, 290–304.

Jbabdi, S., and Johansen-Berg, H. (2011). Tractography: where do we go from here? Brain Connect. *1*, 169–183.

Jbabdi, S., Sotiropoulos, S.N., and Behrens, T.E. (2013). The topographic connectome. Curr. Opin. Neurobiol. *23*, 207–215.

Kaas, J.H. (1997). Topographic maps are fundamental to sensory processing. Brain Res. Bull. *44*, 107–112.

Kobayashi, S., Takayama, C., and Ikeda, Y. (2013). Ontogeny of the brain in oval squid *Sepioteuthis lessoniana* (Cephalopoda: Loliginidae) during the post-hatching phase. J. Mar. Biol. Assoc. U K *93*, 1663–1671.

Koizumi, M., Shigeno, S., Mizunami, M., and Tanaka, N.K. (2016). Three-dimensional brain atlas of pygmy squid, *Idiosepius paradoxus*, revealing the largest relative vertical lobe system volume among the cephalopods. J. Comp. Neurol. *524*, 2142–2157.

Kurniawan, N.D., Richards, K.L., Yang, Z.Y., She, D., Ullmann, J.F.P., Moldrich, R.X., Liu, S., Yaksic, J.U., Leanage, G., Kharatishvili, I., et al. (2014). Visualization of mouse barrel cortex using ex-vivo track density imaging. Neuroimage *87*, 465–475.

Laan, A., Gutnick, T., Kuba, M.J., and Laurent, G. (2014). Behavioral analysis of cuttlefish traveling waves and its implications for neural control. Curr. Biol. *24*, 1737–1742.

Lee, Y.H., Chang, Y.C., Yan, H.Y., and Chiao, C.C. (2013). Early visual experience of background contrast affects the expression of NMDA-like glutamate receptors in the optic lobe of cuttlefish, *Sepia pharaonis*. J. Exp. Mar. Biol. Ecol. *447*, 86–92.

Lin, C.-Y., and Chiao, C.C. (2017). Female choice leads to a switch in oval squid male mating tactics. Biol. Bull. *233*, 219–226.

Lin, C.-Y., Tsai, Y.-C., and Chiao, C.-C. (2017). Quantitative analysis of dynamic body patterning reveals the grammar of visual signals during the reproductive behavior of the oval squid *Sepioteuthis lessoniana*. Front. Ecol. Evol. *5*, 30.

Liscovitch-Brauer, N., Alon, S., Porath, H.T., Elstein, B., Unger, R., Ziv, T., Admon, A., Levanon, E.Y., Rosenthal, J.J., and Eisenberg, E. (2017). Trade-off between transcriptome plasticity and genome evolution in cephalopods. Cell *169*, 191–202.

Liu, C.R., Li, Y.H., Edwards, T.J., Kurniawan, N.D., Richards, L.J., and Jiang, T.Z. (2016). Altered structural connectome in adolescent socially isolated mice. Neuroimage *139*, 259–270.

Liu, T.-H., and Chiao, C.-C. (2017). Mosaic organization of body pattern control in the optic lobe of squids. J. Neurosci. *37*, 768–780.

Liu, Y.-C., Chung, W.-S., Yu, C.-C., Hsu, S.-T., Chan, F.-L., Liu, T.-H., Su, C.-H., Hwu, Y., Marshall, N.J., and Chiao, C.C. (2018). Morphological changes of the optic lobe from late embryonic to adult stages in oval squids *Sepioteuthis lessoniana*. J. Morphol. *279*, 75–85.

Lu, C.-C., and Chung, W.-S. (2017). Guide of the Cephalopods of Taiwan (Huayu Nature Book Trade).

Lynn, C.W., and Bassett, D.S. (2019). The physics of brain network structure, function and control. Nat. Rev. Phys. *1*, 318–332.

Maddock, L., and Young, J.Z. (1987). Quantitative differences among the brains of cephalopods. J. Zool. *212*, 739–767.

Maier-Hein, K.H., Neher, P.F., Houde, J.C., Cote, M.A., Garyfallidis, E., Zhong, J., Chamberland, M., Yeh, F.C., Lin, Y.C., Ji, Q., et al. (2017). The challenge of mapping the human connectome based on diffusion tractography. Nat. Commun. *8*, 1349.

Marshall, N.J., and Messenger, J.B. (1996). Colour-blind camouflage. Nature *382*, 408–409.

Mather, J.A., Griebel, U., and Byrne, R.A. (2010). Squid dances: an ethogram of postures and actions of *Sepioteuthis sepioidea* squid with a muscular hydrostatic system. Mar. Freshw. Behav. Phys. *43*, 45–61.

Meinertzhagen, I.A. (2018). Of what use is connectomics? A personal perspective on the *Drosophila* connectome. J. Exp. Biol. *221*, jeb164954.

Messenger, J.B. (1979). The nervous system of *Loligo*. IV. Peduncle and olfactory lobes. Philos. Trans. R. Soc. Lond. B Biol. Sci. *285*, 275–309.

Miyan, J.A., and Messenger, J.B. (1995). Intracellular recordings from the chromatophore lobes of Octopus. In Cephalopod Neurobiology Neuroscience Studies in Squid, octopus, and Cuttlefish, N.J. Abbott, R. Williamson, and L. Maddock, eds. (Oxford University Press), pp. 415–429.

Nixon, M., and Young, J.Z. (2003). The Brains and Lives of Cephalopods (Oxford University Press).

Novicki, A., Budelmann, B.U., and Hanlon, R.T. (1990). Brain pathways of the chromatophore system in the squid *Lolliguncula brevis*. Brain Res. *519*, 315–323.

Oh, S.W., Harris, J.A., Ng, L., Winslow, B., Cain, N., Mihalas, S., Wang, Q., Lau, C., Kuan, L., Henry, A.M., et al. (2014). A mesoscale connectome of the mouse brain. Nature *508*, 207–214.

Packard, A. (1972). Cephalopods and fish - the limits of convergence. Biol. Rev. Camb. Philos. Soc. *47*, 241–307.

Penfield, W., and Boldrey, E. (1937). Somatic motor and sensory representation in the cerebral cortex of man as studied by electrical stimulation. Brain *60*, 389–443.

Reiter, S., Hulsdunk, P., Woo, T., Lauterbach, M.A., Eberle, J.S., Akay, L.A., Longo, A., Meier-Credo, J., Kretschmer, F., Langer, J.D., et al. (2018). Elucidating the control and development of skin patterning in cuttlefish. Nature *562*, 361–366.

Schnell, A.K., and Clayton, N.S. (2019). Cephalopod cognition. Curr. Biol. *29*, R726–R732.

Shigeno, S., Andrews, P.L.R., Ponte, G., and Fiorito, G. (2018). Cephalopod brains: an overview of current knowledge to facilitate comparison with vertebrates. Front. Physiol. *9*, 952.

Shigeno, S., Ogura, A., Mori, T., Toyohara, H., Yoshida, T., Tsuchida, S., and Fujikura, K. (2014). Sensing deep extreme environments: the receptor cell types, brain centers, and multi-layer neural packaging of hydrothermal vent endemic worms. Front. Zool. *11*, 82.

Shigeno, S., and Ragsdale, C.W. (2015). The gyri of the octopus vertical lobe have distinct neurochemical identities. J. Comp. Neurol. *523*, 1297–1317.

Shigeno, S., Tsuchiya, K., and Segawa, S. (2001). Embryonic and paralarval development of the central nervous system of the loliginid squid *Sepioteuthis lessoniana*. J. Comp. Neurol. *437*, 449–475.

Shih, C.T., Sporns, O., Yuan, S.L., Su, T.S., Lin, Y.J., Chuang, C.C., Wang, T.Y., Lo, C.C., Greenspan, R.J., and Chiang, A.S. (2015). Connectomics-based analysis of information flow in the Drosophila brain. Curr. Biol. *25*, 1249–1258.

Shomrat, T., Zarrella, I., Fiorito, G., and Hochner, B. (2008). The octopus vertical lobe modulates short-term learning rate and uses LTP to acquire long-term memory. Curr. Biol. *18*, 337–342.

Sinakevitch, I., Douglass, J.K., Scholtz, G., Loesel, R., and Strausfeld, N.J. (2003). Conserved and convergent organization in the optic lobes of insects and isopods, with reference to other crustacean taxa. J. Comp. Neurol. *467*, 150–172.

Sotiropoulos, S.N., and Zalesky, A. (2019). Building connectomes using diffusion MRI: why, how and but. NMR Biomed. *32*, e3752.

Strausfeld, N.J. (1980). The Golgi method: Its application to the insect nervous system and the phenomenon of stochastic impregnation. In Neuroanatomical Techniques, N.J. Strausfeld and T.A. Miller, eds. (Springer), pp. 131–203.

Strausfeld, N.J. (2005). The evolution of crustacean and insect optic lobes and the origins of chiasmata. Arthropod Struct. Dev. *34*, 235–256.

Strausfeld, N.J., Ma, X., and Edgecombe, G.D. (2016). Fossils and the evolution of the arthropod brain. Curr. Biol. *26*, R989–R1000.

Strugnell, J., Jackson, J., Drummond, A.J., and Cooper, A. (2006). Divergence time estimates for major cephalopod groups: evidence from multiple genes. Cladistics *22*, 89–96.

Strugnell, J., Norman, M., Jackson, J., Drummond, A.J., and Cooper, A. (2005). Molecular phylogeny of coleoid cephalopods (Mollusca: cephalopoda) using a multigene approach; the effect of data partitioning on resolving phylogenies in a Bayesian framework. Mol. Phylogenet. Evol. *37*, 426–441.

Suarez, R., Paolino, A., Fenlon, L.R., Morcom, L.R., Kozulin, P., Kurniawan, N.D., and Richards, L.J. (2018). A pan-mammalian map of interhemispheric brain connections predates the evolution of the corpus callosum. Proc. Natl. Acad. Sci. U S A *115*, 9622–9627.

Sugimoto, C., and Ikeda, Y. (2012). Ontogeny of schooling behavior in the oval squid *Sepioteuthis lessoniana*. Fish. Sci. *78*, 287–294.

Sutherland, N.S., Mackintosh, J., and Mackintosh, N.J. (1963). The visual discrimination of reduplicated patterns by octopus. Anim. Behav. *11*, 106–110.

Sweeney, A.M., Haddock, S.H., and Johnsen, S. (2007). Comparative visual acuity of coleoid cephalopods. Integr. Comp. Biol. *47*, 808–814.

Takemura, S., Aso, Y., Hige, T., Wong, A., Lu, Z.Y., Xu, C.S., Rivlin, P.K., Hess, H., Zhao, T., Parag, T., et al. (2017). A connectome of a learning and memory center in the adult Drosophila brain. Elife *6*, e26975.

Thomas, C., Ye, F.Q., Irfanoglu, M.O., Modi, P., Saleem, K.S., Leopold, D.A., and Pierpaoli, C. (2014). Anatomical accuracy of brain connections derived from diffusion MRI tractography is inherently limited. Proc. Natl. Acad. Sci. U S A *111*, 16574–16579.

Valverde, F. (1998). Golgi Atlas of the Postnatal Mouse Brain (Springer-Verlag).

Vecchione, M., Brakoniechki, T.F., Natsukari, Y., and Hanlon, R.T. (1998). A provisional generic classification of the family Loliginidae. In Cephalopod International Advisory Council, Voss., ed. (Smithsonian Institution Press), pp. 215–222.

Wells, M.J. (1963). Taste by touch: some experiments with octopus. J. Exp. Biol. *40*, 187–193.

Wells, M.J., and Wells, J. (1957). The effect of lesions to the vertical and optic lobes on tactile discrimination in *Octopus*. J. Exp. Biol. *34*, 378–393.

White, J.G., Southgate, E., Thomson, J.N., and Brenner, S. (1986). The structure of the nervous system of the nematode *Caenorhabditis elegans*. Philos. Trans. R. Soc. Lond. B Biol. Sci. *314*, 1–340.

Wild, E., Wollesen, T., Haszprunar, G., and Hess, M. (2015). Comparative 3D microanatomy and histology of the eyes and central nervous systems in coleoid cephalopod hatchlings. Org. Divers. Evol. *15*, 37–64.

Wollesen, T., Loesel, R., and Wanninger, A. (2009). Pygmy squids and giant brains: mapping the complex cephalopod CNS by phalloidin staining of vibratome sections and whole-mount preparations. J. Neurosci. Methods *179*, 63–67.

Wollesen, T., Sukhsangchan, C., Seixas, P., Nabhitabhata, J., and Wanninger, A. (2012). Analysis of neurotransmitter distribution in brain development of benthic and pelagic octopod cephalopods. J. Morphol. *273*, 776–790.

Young, J.Z. (1961). Learning and discrimination in the octopus. Biol. Rev. Camb. Philos. Soc. *36*, 32–96.

Young, J.Z. (1971). The Anatomy of the Nervous System of Octopus vulgaris (Clarendon Press).

Young, J.Z. (1974). The central nervous system of *Loligo*. I. The optic lobe. Philos. Trans. R. Soc. Lond. B Biol. Sci. *267*, 263–302.

Young, J.Z. (1976). The nervous system of *Loligo*. II. Subesophageal centers. Philos. Trans. R. Soc. Lond. B Biol. Sci. *274*, 101–167.

Young, J.Z. (1977). The nervous system of *Loligo*. III. Higher motor centers - the basal supraesophageal lobes. Philos. Trans. R. Soc. Lond. B Biol. Sci. *276*, 351–398.

Young, J.Z. (1979). The nervous system of *Loligo*. V. The vertical lobe complex. Philos. Trans. R. Soc. Lond. B Biol. Sci. *285*, 311–354.

Young, R.E. (1964). The Anatomy of the Vampire Squid, Master (University of Sothern California).

Ziegler, A., Bock, C., Ketten, D.R., Mair, R.W., Mueller, S., Nagelmann, N., Pracht, E.D., and Schröder, L. (2018). Digital three-dimensional imaging techniques provide new analytical pathways for malacological research. Am. Malacol. Bull. *36*, 248–273.

Zullo, L., Sumbre, G., Agnisola, C., Flash, T., and Hochner, B. (2009). Nonsomatotopic organization of the higher motor centers in octopus. Curr. Biol. *19*, 1632–1636.

ISCI, Volume *23*

Supplemental Information

Toward an MRI-Based Mesoscale Connectome of the Squid Brain

Wen-Sung Chung, Nyoman D. Kurniawan, and N. Justin Marshall

Supplemental information

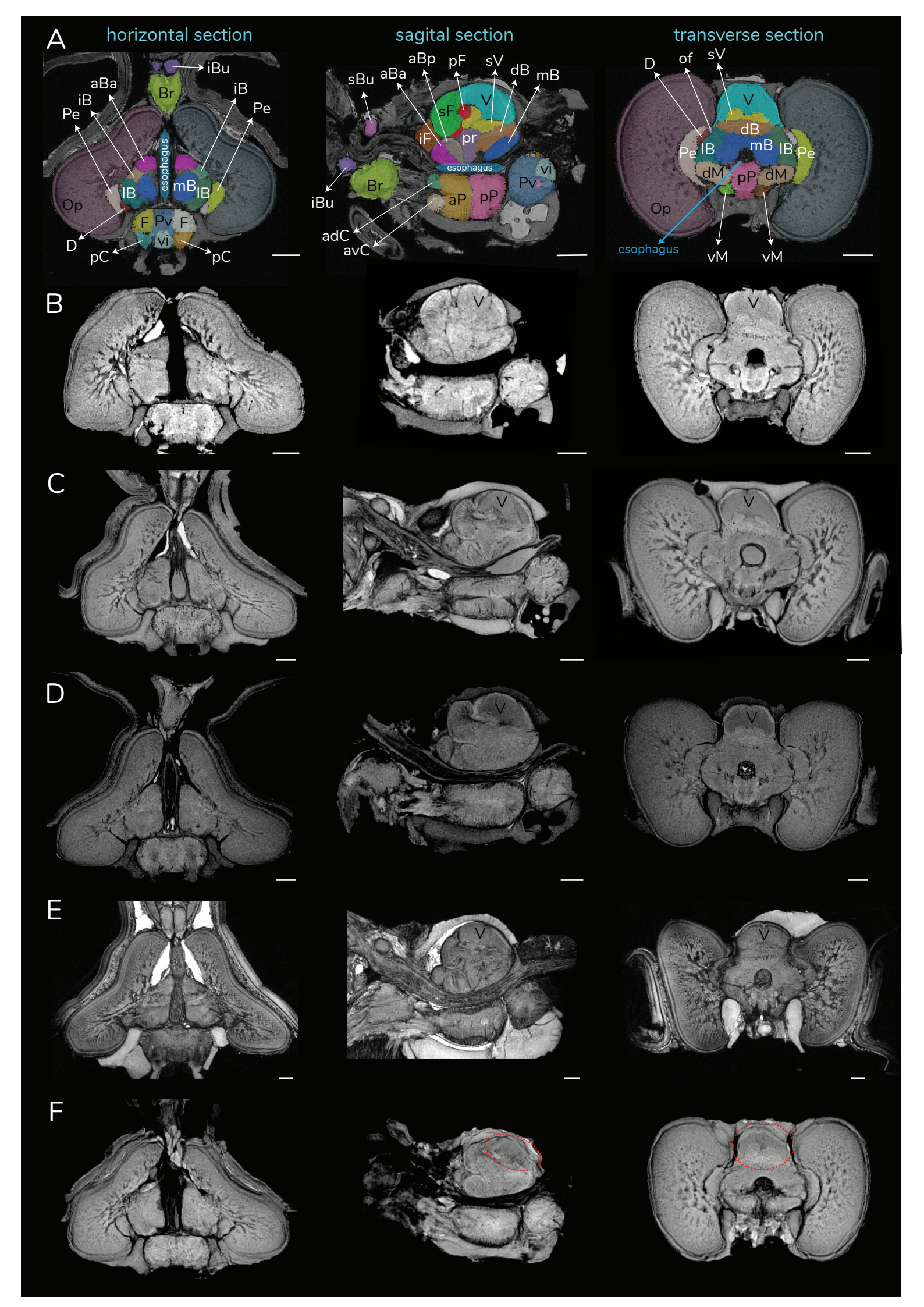
A
horizontal section
sagital section
transverse section
iBu
aBa
iB
Pe
Br
esophagus
lB
mB
Op
F
Pv
vi
D
pC
aBp
pF
sV
dB
mB
sBu
sF
V
iF
pr
vi
Pv
aP
pP
adC
avC
of
dM
vM
B
C
D
E
F

Figure S1 Magnetic resonance imagery of the squid brain (Related to Figures 1, 5A, 5D and Table S1)

(A-E) High-resolution magnetic resonance histology of the squid brain from 5 individuals (isotropic resolution 30 μm) showing changes of lobe morphology during ontogeny. **(F)** The averaged squid brain was computed using Advanced Neuroimaging Tools (ANTs) with 4 similar sized squid brains (A-D). After long computation (ca. 89 h), the boundaries between the lobes of this averaged squid brain became more blurred than individual MR images obtained from each individual (e.g. vertical lobe), resulting in challenges in lobe segmentation.

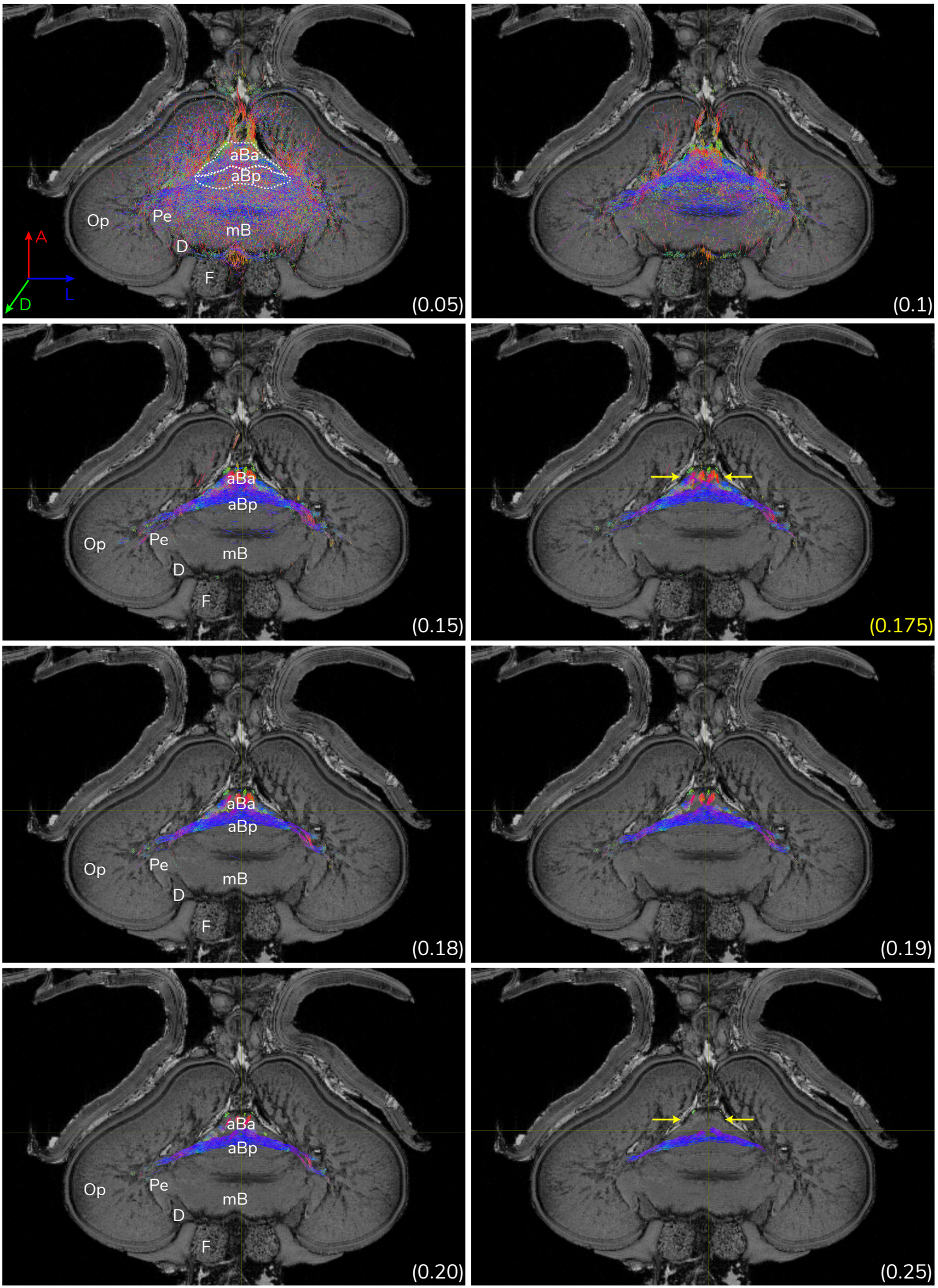
aBa
aBp
Op
Pe
mB
D
F
A
L
D
(0.05)
(0.1)
(0.15)
(0.175)
(0.18)
(0.19)
(0.20)
(0.25)

Figure S2 Comparisons of probabilistic tractography streamlines reconstructed by varying the tract acceptance thresholds (Related to Figures 2D, 2E, 5A, 6-8)

A series of examples of tractography streamlines derived from an entire anterior anterior basal lobe (aBa) reconstructed using different cut-off parameters of tract acceptance between 0.05 and 0.25 (horizontal section). The color-coded neural tracts show the orientation of neural bundles equivalent to the body axes. A, anterior; D, dorsal; L, lateral. Given higher thresholds (from 0.05 to 0.15), the algorithm significantly filtered out erroneous streamlines which appeared in the anterior posterior basal lobe (aBp), dorsolateral lobe (D), median basal lobe (mB), optic lobe (Op) and peduncle lobe (Pe). With the threshold over 0.18, both sensitivity and specificity of the tractography erroneously removed the streamlines showing the neural bundles that appeared in histology (e.g. Figure 2G-H in the main text), giving false negative results. For instance, using the cut-off value 0.25, most inter-lobed connections between aBa and aBp and the pair of contralateral tracts (e.g. Figures 2G-H in the main text) derived from the anterior median lobules of aBa were completely removed. Yellow arrows indicated the differentials of tractography (intensity and streamlines) between two thresholds (cut-off 0.175 versus 0.25).

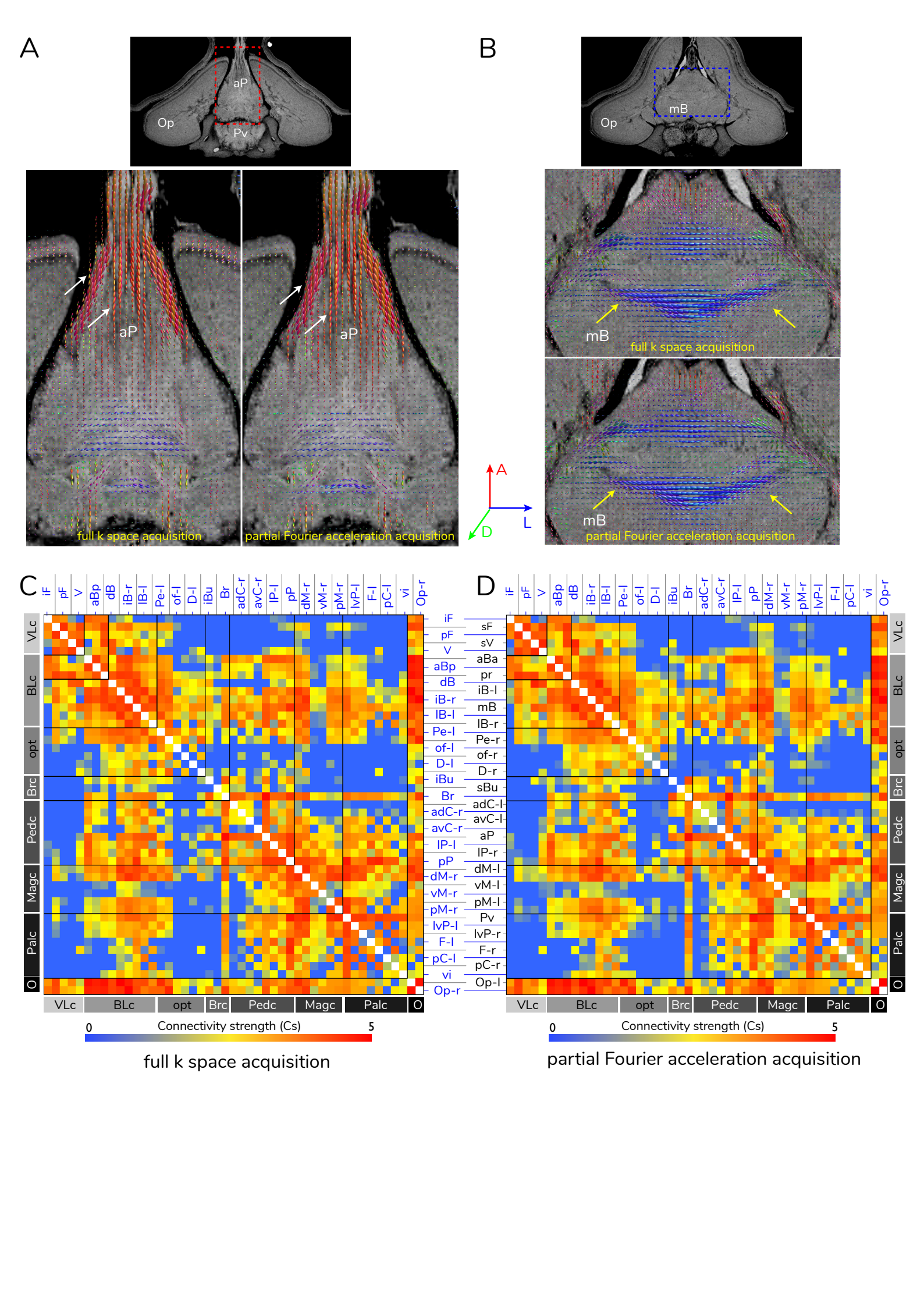
A
aP
Op
Pv
aP
aP
full k space acquisition
partial Fourier acceleration acquisition
B
mB
Op
mB
full k space acquisition
mB
partial Fourier acceleration acquisition
A
L
D
C
iF pF V aBp dB iB-r lB-l Pe-l of-l D-l iBu Br adC-r avC-r lP-l pP dM-r vM-r pM-r lvP-l F-l pC-l vi Op-r
VLc BLc opt Brc Pedc Magc Palc O
iF pF V aBp dB iB-r lB-l Pe-l of-l D-l iBu Br adC-r avC-r lP-l pP dM-r vM-r pM-r lvP-l F-l pC-l vi Op-r
sF sV aBa pr iB-l mB lB-r Pe-r of-r D-r sBu adC-l avC-l aP lP-r dM-l vM-l pM-l Pv lvP-r F-r pC-r Op-l
VLc BLc opt Brc Pedc Magc Palc O
0 Connectivity strength (Cs) 5
full k space acquisition
D
iF pF V aBp dB iB-r lB-l Pe-l of-l D-l iBu Br adC-r avC-r lP-l pP dM-r vM-r pM-r lvP-l F-l pC-l vi Op-r
VLc BLc opt Brc Pedc Magc Palc O
VLc BLc opt Brc Pedc Magc Palc O
0 Connectivity strength (Cs) 5
partial Fourier acceleration acquisition

Figure S3 Comparisons between full and partial Fourier acceleration acquisitions (Related to Figure 2D-E, 5A, S4)

(A-B) A high degree of similarity in fiber orientation distribution (FOD) between full k-space acquisition and partial Fourier acceleration acquisition procedures of the squid tracts (ML: 48.32mm). **(A)** Brachial nerves (white arrows). **(B)** Optic nerves (yellow arrows). The color-coded FODs show the orientation of neural bundles equivalent to the body axes. A, anterior; D, dorsal; L, lateral. **(C-D)** A high degree of similarity (96.48%) in the connectivity matrices between the two imaging procedures.

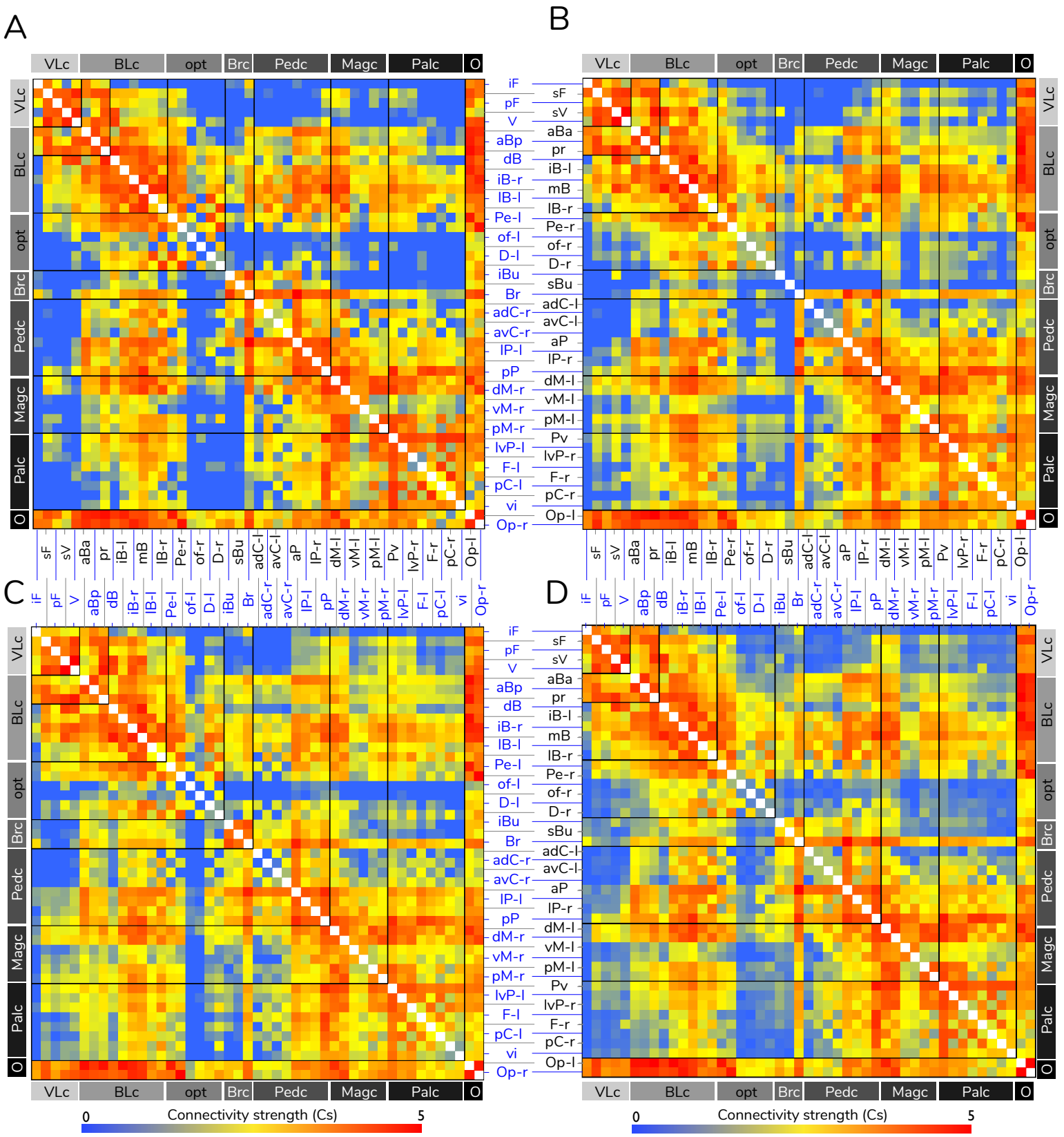
A
B
C
D
VLc
BLc
opt
Brc
Pedc
Magc
Palc
O
iF
sF
pF
sV
V
aBa
aBp
pr
dB
iB-l
iB-r
mB
lB-l
lB-r
Pe-l
Pe-r
of-l
of-r
D-l
D-r
iBu
sBu
Br
adC-l
adC-r
avC-l
avC-r
aP
lP-l
lP-r
pP
dM-l
dM-r
vM-l
vM-r
pM-l
pM-r
Pv
lvP-l
lvP-r
F-l
F-r
pC-l
pC-r
vi
Op-l
Op-r
0
Connectivity strength (Cs)
5

Figure S4 Connectivity matrices of the squid brain (Related to Figures 5A, 5C, 5D)

(A) Probabilistic tractography connectivity matrix of the smallest squid brain (ML: 55mm). The heat map indicates $\log_{10}$-transfered connection strength (*Cs*). **(B)** The connectivity matrix of the second largest individual (ML: 58.28mm) **(C)** The connectivity matrix of the largest specimen (ML: 113mm) **(D)** An averaged probabilistic tractography connectivity matrix of 5 individuals.

	Squid 1		Squid 2		Squid 3		Squid 4		Squid 5	
	ML:55mm MRI: 5.45h dMRI: 20.9h		ML: 40.28mm MRI: 4.13h dMRI: 22.2h		ML:48.32mm MRI: 5.2h dMRI: 22.7h dMRI*: 33.8h		ML:58.25mm MRI: 7.4h dMRI: 28.8h dMRI*: 40.8h		ML:113mm MRI: 7.8h dMRI: 32.5h	
Lobe	**Volume (mm^3)**	**lobe/CNS (%)**	**Volume (mm^3)**	**lobe/CNS (%)**	**Volume (mm^3)**	**lobe/CNS (%)**	**Volume (mm^3)**	**lobe/CNS (%)**	**Volume (mm^3)**	**lobe/CNS (%)**
Inferior frontal (iF)	0.1889	0.16	0.2187	0.16	0.2855	0.13	0.3811	0.15	0.9839	0.17
Superior frontal (sF)	1.1068	0.91	1.1463	0.83	1.6657	0.77	2.3027	0.90	4.5060	0.77
Posterior frontal (pF)	0.1286	0.11	0.1176	0.09	0.2819	0.13	0.4008	0.16	0.6185	0.11
Subvertical (sV)	0.7841	0.65	1.1628	0.84	1.4441	0.67	1.8946	0.74	5.4930	0.94
Vertical (V)	2.6887	2.22	3.5924	2.61	5.6126	2.59	5.6473	2.21	19.0700	3.27
Anterior anterior basal (aBa)	0.7926	0.65	1.0541	0.76	1.4925	0.69	1.9928	0.78	2.6510	0.46
Anterior posterior basal (aBp)	0.5726	0.47	0.6169	0.45	0.8930	0.41	1.1559	0.45	5.2790	0.91
Precommisural (pr)	0.8318	0.69	0.8046	0.58	1.1945	0.55	1.6478	0.64	3.2900	0.56
Dorsal basal (dB)	0.9241	0.76	0.7491	0.54	0.8273	0.38	1.4868	0.58	3.5850	0.62
Interbasal-L (iB-l)	0.2251	0.19	0.5153	0.37	0.7733	0.36	0.6923	0.27	0.6270	0.11
Interbasal-R (iB-r)	0.2309	0.19	0.4756	0.35	0.7874	0.36	0.9045	0.35	0.6465	0.11
Medial basal (mB)	1.4134	1.17	2.2470	1.63	3.3964	1.57	3.9957	1.56	10.9200	1.88
Lateral basal-L (lB-l)	0.5808	0.48	0.4566	0.33	0.6433	0.30	0.8737	0.34	1.9140	0.33
Lateral basal-R (lB-r)	0.5650	0.47	0.4353	0.32	0.6058	0.28	0.8343	0.33	1.8820	0.32
Peduncle-L (Pe-l)	0.7330	0.61	0.6180	0.45	1.1712	0.54	1.1126	0.44	2.2150	0.38
Peduncle-R (Pe-r)	0.7269	0.60	0.6510	0.47	1.1647	0.54	1.1178	0.44	2.5670	0.44
Olfactory-L (ol-l)	0.0102	0.01	0.0068	0.00	0.0165	0.01	0.0257	0.01	0.0402	0.01
Olfactory-R (ol-r)	0.0103	0.01	0.0092	0.01	0.0120	0.01	0.0225	0.01	0.0316	0.01
Dorsolateral-L (D-l)	0.1902	0.16	0.1751	0.13	0.2232	0.10	0.2449	0.10	0.8524	0.15
Dorsolateral-R (D-r)	0.1939	0.16	0.1852	0.13	0.2295	0.11	0.2982	0.12	0.9235	0.16
Inferior buccal (iBu)	0.2279	0.19	n.a.	n.a.	0.4220	0.19	n.a.	n.a.	2.5860	0.44
Superior buccal (sBu)	0.2639	0.22	n.a.	n.a.	0.4896	0.23	n.a.	n.a.	1.5070	0.26
Brachial (Br)	1.3953	1.15	n.a.	n.a.	2.2037	1.02	2.6625	1.04	12.5700	2.16
Anterior dorsal chromatophore-L (adC-l)	0.0540	0.04	0.0211	0.02	0.0740	0.03	0.1827	0.07	0.3294	0.06
Anterior dorsal chromatophore-R (adC-r)	0.0814	0.07	0.0213	0.02	0.0639	0.03	0.1653	0.06	0.3522	0.06
Anterior ventral chromatophore-L (avC-l)	0.1101	0.09	0.0550	0.04	0.0645	0.03	0.1344	0.05	0.2965	0.05
Anterior ventral chromatophore-R (adC-r)	0.1045	0.09	0.0463	0.03	0.0699	0.03	0.1204	0.05	0.2957	0.05
Anterior pedal (aP)	1.2150	1.00	1.6027	1.16	2.7655	1.27	2.6186	1.02	8.6830	1.49
Lateral pedal-L (lP-l)	0.2962	0.24	0.3556	0.26	0.4775	0.22	0.5774	0.23	1.1820	0.20

Lateral pedal-R (lP-r)	0.2609	0.22	0.3330	0.24	0.4505	0.21	0.5746	0.22	1.2490	0.21
Posterior pedal (pP)	1.2783	1.06	1.9455	1.41	2.7578	1.27	3.4689	1.36	10.3200	1.77
Dorsal magnocellular-L (dM-l)	0.4793	0.40	0.5681	0.41	0.8900	0.41	0.9731	0.38	2.4230	0.42
Dorsal magnocellular-R (dM-r)	0.4820	0.40	0.5274	0.38	0.8481	0.39	0.9595	0.38	2.5320	0.43
Ventral magnocellular-L (vM-l)	0.0668	0.06	0.0694	0.05	0.0999	0.05	0.0937	0.04	0.2874	0.05
Ventral magnocellular-R (vM-r)	0.0675	0.06	0.0725	0.05	0.0887	0.04	0.0939	0.04	0.3040	0.05
Posterior magnocellular-L (pM-l)	0.2930	0.24	0.3252	0.24	0.4220	0.19	0.5069	0.20	1.2070	0.21
Posterior magnocellular-R (pM-r)	0.2359	0.19	0.3010	0.22	0.4162	0.19	0.4601	0.18	1.3170	0.23
Palliovisceral (Pv)	1.2039	0.99	1.4396	1.04	2.5679	1.18	3.5454	1.39	8.3750	1.44
Lateral ventral palliovisceral-L (lvP-l)	0.1499	0.12	0.2676	0.19	0.4066	0.19	0.3445	0.13	1.0230	0.18
Lateral ventral palliovisceral-R (lvP-r)	0.1320	0.11	0.2682	0.19	0.4349	0.20	0.3057	0.12	1.0380	0.18
Fin-L (F-l)	0.4874	0.40	0.6723	0.49	0.9596	0.44	0.9558	0.37	3.5120	0.60
Fin-R (F-r)	0.4636	0.38	0.5977	0.43	0.9537	0.44	1.0437	0.41	3.4460	0.59
Posterior chromatophore-L (pC-l)	0.2334	0.19	0.1586	0.12	0.3402	0.16	0.4398	0.17	2.0920	0.36
Posterior chromatophore-R (pC-r)	0.2289	0.19	0.0821	0.06	0.3380	0.16	0.4581	0.18	2.2320	0.38
Visceral (vi)	0.1907	0.16	0.4086	0.30	0.4431	0.20	0.3093	0.12	1.2300	0.21
Optic-L (O-l)	48.8531	40.37	56.2580	40.83	87.4925	40.32	102.0040	39.89	221.0000	37.95
Optic-R (O-r)	49.2619	40.71	56.1566	40.75	87.7371	40.43	105.6950	41.33	222.9000	38.27
CNS total volume	**121.0145**		**137.7907**		**216.9976**		**255.7251**		**582.3848**	

Table S1 Estimates of lobe volume of juvenile squid (Related to Figure 1G-H, 5D)

* indicates that two specimens were scanned using the full k-space acquisition procedure.

	***Young** (1974,1976,1977,1979)* ***Messenger** (1979)*	***Wild et al** (2015)*	***Shigeno et al** (2001)* ***Kobayashi et al** (2103)*	***Current study***
Loliginids	*Alloteuthis subulata**ψ *Loligo vulgaris**ψ *Loligo pealeii** σ *Loligo forbesi*ψ *Sepioteuthis sp.* σ mostly post-hatchlings	*Loligo vulgaris*ψ hatchling	*Sepioteuthis lessoniana* ρ embryos, hatchlings, post-hatchlings (3-55d), juveniles	*Sepioteuthis lessoniana* ρ juveniles
Methods	Silver staining (Cajal's & Golgi-Kopsch method	Semi-thin sections with Richardson staining	Conventional histology (H&E staining); Silver staining (Cajal's method)	Modified Cajal-Golgi silver staining; multi-colour neural tracers (NeuroVue); Magnetic resonance imaging (MRI); High angular resonance diffusion imaging (HARDI); Probabilistic tractography
Results	Gross brain anatomy (morphological analysis); Description of various neurons; Lobe-related tracts	Gross brain anatomy (morphological and volumetric analysis)	Gross brain anatomy (morphological analysis); Ontogenetic development of brain (neuropils and tracts);	Gross brain anatomy (morphological and volumetric analysis); 3D neural tracts; Brain-wide neural connectivity matrix
Notes	Continuous influence in shaping our knowledge toward the gross anatomy and connectivity of the squid brain by these 5 pioneering studies.	3D microanatomy of the squid brain.	Age-dependent heterogeneity in formation of neuropils and neural connectivity in the lobes of squid brain.	A new neural connection map reveals 153 new lobe-to-lobe tracts, leading new proposed functional circuits.

Table S2 List of the loliginid squid brain anatomical studies (Related to Figure 1, Table 1)

* indicates that the three species were dominantly used in these 5 studies.

ψ indicates that the distribution of the species in the eastern North Atlantic Ocean; σ in the western North Atlantic Ocean; ρ in the Indo-Pacific Ocean.

Key Resource Table

REAGENT or RESOURCE	SOURCE	IDENTIFIER
Experimental animal		
Squid: *Sepioteuthis lessoniana*	Wild (Moreton Bay, Brisbane)	N/A
Software and Algorithms		
Paravision 6	Preclinical MRI software, Bruker Biospin	Bruker
MRtrix3	version 3.0_RC3, open-source software	http://www.mrtrix.org/
ITK-SNAP	version 3.6.0, open-source software	http://www.itksnap.org/
Fiji	NIH	https://fiji.sc/
ANTs	Advanced normalization tools	http://stnava.github.io/ANTs/
Zen	Zeiss	https://www.zeiss.com/microscopy/int/products/microscope-software/zen.html
Deposited Data		
Squid Brain MRI images	DOI: 10.17632/pwkh3s2t33.1	Mendeley Data
Chemicals		
Glutaraldehyde	Electron Microscopy Science	Cat# 16220
Paraformaldehyde	Electron Microscopy Science	Cat# 15170
DAPI	Sigma-Aldrich	Cat# D9542-5MG
Durcupan resin	Sigma-Aldrich	Cat# 44610-1EA
Osmium tetroxide	Sigma-Aldrich	Cat# 75632-5ML
Potassium dichromate	Sigma-Aldrich	Cat# 207802-100
Silver nitrate	Sigma-Aldrich	Cat# 209139-25G
Magnesium chloride	Chem-Supply	Cat# MA029-500G
Sucrose	Chem-Supply	Cat# SA030-500G
NeuroVue (jade)	Polysciences Incorporated	Cat# 24837
NeuroVue (red)	Polysciences Incorporated	Cat# 24835
Optimal cutting temperature compound	Tissue-Tek	Cat# IA018
Magnevist	Bayer	Cat# NDC 50419-188-82
Fomblin	Solvay	Cat# LVOF066K

Transparent Methods

Sample collection and preparation

Oval squid, *Sepioteuthis lessoniana,* (mantle length (ML) 13 - 113 mm) were collected using a seine net (water depth 1-3 m) close to Moreton Bay Research Station, Stradbroke Island, Queensland, Australia. The maintenance and experimental protocol used here were covered by animal ethics permit (QBI/236/13/ARC/US AIRFORCE & QBI/304/16). Animals were anesthetized in cold seawater mixed with 2% $MgCl_2$ (Chem-Supply, Australia) and sacrificed by an overdose of $MgCl_2$ prior to the histological preparation of neural tracing and magnetic resonance imaging of the squid brain (Chung and Marshall, 2017).

Method Details

Modified Cajal-Golgi rapid silver impregnation

This classical silver staining method is an effective tool in screening populations of neurons and used here to validate the probabilistic tractography we established in this study. With manipulations of fixatives, osmolality by adjusted sucrose, incubation time and concentration of the silver nitrate solution, over 1000 silver stained neural bundles were obtained from 40 juvenile squid (ML = 13-25 mm).

The protocol of Cajal-Golgi rapid impregnation for the squid brain was modified from the standard protocol for the insect brain developed by Strausfeld (1980) and was in most respects similar to the procedures of Cajal (1917) as follows: (1) The brain was dissected in freshly-prepared fixative consisting of 1 part of 25% glutaraldehyde (EM grade, Electron Microscopy Sciences, Hatfield, USA) and 5 parts of 2.5% potassium dichromate solution (Sigma-Aldrich, USA) in 12% sucrose (Chem-Supply, Australia). The isolated brain was then placed in a light-sealed container filled with fresh fixative for another 24 hours at room temperature. (2) The isolated brain was transferred into the second incubation solution consisting of 2.5% potassium dichromate (99 parts) with 1% osmium tetroxide (1 part) (Sigma-Aldrich, USA) for 5-7 days followed by 0.75% silver nitrate (Sigma-Aldrich, USA) for 3 days incubation at room temperature. The impregnated brain was soaked briefly in distilled water and cleaned using an ultrasonic bath (XUBA1, Grant Instrument, USA) for 5-10 minutes to remove silver crystals

(silver chromate) on the surface of the sample. (3) Where necessary, repeat the second step. (4) Samples were dehydrated and embedding in Durcupan resin (Sigma-Aldrich, USA) following the protocol developed by Strausfeld (1980). (5) The samples were cut into 30-40 μm slices for microscopy using a microtome (RM2235, Leica, Germany). (6) Slice images were compared to tractography virtual slices closest to the histological sections (see Figures 2B, 2G, 3).

Multi-color fluorescent neural tracers

Five juvenile squid (ML = 13-25 mm) were fixed using a modified transcardial perfusion protocol developed by Abbott et al. (1985) using 4% paraformaldehyde (PFA) (EM grade, Electron Microscopy Sciences, Hatfield, USA) mixed with 0.1M phosphate buffer solution (PBS) with the rate of perfusion set to 2.5 ml per minute. The perfusion proceeded until 1 ml fixative per gram of squid was used. Subsequently the muscle, skin and connective tissues around the brain were removed and the specimen was soaked in 4% PFA mixed with 0.1M PBS for 6-10 hrs prior to loading the fluorescent dyes close to the neural tracts of interest. The lipophilic dye tracers NeuroVue (Polysciences Incorporated, Warrington, USA) red and jade were used for neural tracing according to the manufacturer's protocol with some modifications. Fine slivers of coated dye filters were inserted at the selected regions after small incisions in the brain and nerves were made, the cut-loading process (see Figure 4A). NeuroVue-treated brains were then placed in a light-sealed container filled with fresh 0.1% PFA fixative in 0.1M PBS at room temperature and the dyes were allowed to diffuse along the neural membranes for 40-80 days. The brains were embedded in Optimal Cutting Temperature compound (OCT - Tissue-Tek, Sakura Finetek, USA) plus 10% sucrose for cryosectioning (25 μm thickness) at -20ºC (CM 1100, Leica, Germany). The slice was stained with DAPI (Sigma-Aldrich, USA) to visualize nuclei and mounted in glycerol prior to imaging.

Microscopy

Both silver impregnation and fluorescent dye tracing samples were imaged using Zeiss Axio imager (Zeiss, Germany) at the advanced microscopy facility of the Queensland Brain Institute. Additional processing of images for image stitching and brightness adjustment was performed using Zen software (Zeiss, Germany) and open-source image analysis software Fiji (Schindelin et al., 2012).

Contrast-enhanced magnetic resonance imagery (MRI) and high angular resolution diffusion magnetic resonance imagery (HARDI) data acquisition

Specimens for MR imaging were fixed using the same transcardial perfusion protocol described above. The perfusion fixed squid were soaked into 4 % PFA mixed with 0.1 M PBS overnight to reduce morphological deformation of the brain. Intact brain and eyeballs were then isolated and repeatedly rinsed with 0.1 M PBS to minimize fixative residue. Finally, the preserved sample was soaked into 0.1 M PBS containing magnetic resonance imaging (MRI) contrast agent, 0.2% ionic Gd-DTPA (Magnevist) (Bayer, Leverkusen, Germany), for 24-48 hours to enhance image contrast (Chung and Marshall, 2017).

Five contrast-enhanced brains were imaged (isotropic resolution = 30 μm) following the protocol developed by Chung and Marshall (2017). The contrast-enhanced specimen was placed into fomblin-filled (Fomblin oil, Y06/6 grade, Solvay, USA) container to prevent dehydration and then vacuumed for 10-15 minutes to remove air bubbles trapped inside esophagus or brain lobes. The container was then placed in a custom-built surface acoustic wave coil (15 mm diameter) (M2M Imaging, Brisbane, Australia). Both high resolution MR structural images and high angular resolution diffusion images (HARDI) were acquired using a 16.4 Tesla (700 MHz) vertical wide-bore microimaging system (interfaced to an AVANCE I spectrometer running imaging software Paravision 6 (Bruker Biospin, Karlsruhe, Germany) in the Centre for Advanced Imaging at the University of Queensland. Imaging was performed at a temperature of 22 ± 0.1 ºC using a circulating water-cooling system. Three dimensional high resolution structural images were acquired using fast low angle shot (FLASH) with the following parameters and based on Chung and Marshall (2017): echo time (TE) / repetition time (TR) = 14/40 ms, average = 4, flip angle (FA) = 30, field of view (FOV) = 15.0 x 13.8 x 12.5 mm - 20.0 x 13.3 x 17.1 mm for 5 squid individuals, 30 μm isotropic resolution. Total acquisition time for one brain was 4.1-7.8 h.

After FLASH imaging, three-dimensional HARDI was consecutively acquired with the following parameters: repetition time 300 ms, echo time 22 ms, 30 direction diffusion encoding with b-value = 3000 s/mm^2, two b0 images acquired without diffusion weighting and 80 μm isotropic resolution with full k-space acquisition (n = 2) or 1.5 partial Fourier acceleration acquisition (n = 5) in the phase dimensions (Liu et al., 2016). Total acquisition time for one brain was 20.9 - 40.8 h.

HARDI image analyses and construction of multi-scale brain networks

Estimates of lobe volume and construction of tractography

The first step in constructing a structural connection network is to define regions of interest (ROIs) as nodes (see Figures 1, S1). Using anatomical information to improve the accuracy of HARDI streamlines tractography (Smith et al., 2012, Girard et al., 2014) and the ROIs in this study were defined as the squid brain lobes based on the published anatomical studies (Young, 1974, Young, 1976, Young, 1977, Young, 1979, Messenger, 1979, Shigeno et al., 2001, Nixon and Young, 2003, Kobayashi et al., 2013, Wild et al., 2015, Koizumi et al., 2016, Chung and Marshall, 2017). Five ex-vivo MRI-based atlases of juvenile coastal squid, *S. lessoniana*, (ML: 40.28 - 113 mm) were utilised to create the parcellation of the brain which was then manually segmented into 47 ROIs using MRtrix3 (version 3.0_RC3, open-source software, http://www.mrtrix.org/) (Tournier et al., 2012) and then estimates of lobe volume were calculated using ITK-SNAP (version 3.6.0, open-source software, http://www.itksnap.org/) (Yushkevich et al., 2006). Additionally, the averaged squid MR images were transformed using the 4 small-sized squid by Advanced Normalization Tools (ANTs, http://stnava.github.io/ANTs/) (Liu et al., 2016) (Figure S1).

The second step of neural connectivity construction was to compute the structural connections, also known as the edges, which represent pairwise relationships between nodes (lobes) via probabilistic tractography (Descoteaux et al., 2009, Liu et al., 2016). Probabilistic tractography was performed using scripts based on MRtrix3, using procedures also used in the established protocols for the mouse and human brain (Descoteaux et al., 2009, Smith et al., 2012, Calamante et al., 2012, Girard et al., 2014, Liu et al., 2016) along with additive modifications developed in this study as detailed below.

Using the known squid neural pathways described by Young and his colleagues (Young, 1974, Young, 1976, Young, 1977, Young, 1979, Messenger, 1979, Nixon and Young, 2003), the sensitivity (the ability to detect true connections) and specificity (the ability to avoid false connections) of the squid tractography were tested using a combination of parameters and algorithms as follows: (1) The analysis includes constrained spherical deconvolution (CSD) to model fiber orientation distribution (FOD) in each voxel (Tournier et al., 2007, Descoteaux et

al., 2009) (Figures 2D-E, S3-4). (2) Probabilistic fiber tracking was performed using second order integration over the fiber orientation distribution (FOD) algorithm and the tracking was terminated using different threshold of FOD amplitude between 0.05 (default) and 0.25 (Figure S2). Tracts were generated independently for each pair of ROIs (10 streamlines per voxel). (3) Selected lobes (e.g. basal, peduncle, magnocellular, and pedal lobes) and their fiber geometries obtained from histology (using either our Golgi impregnation or neural fluorescent tracers in this study combined with the work by Young and his colleagues) (Young, 1974, Young, 1976, Young, 1977, Young, 1979, Messenger, 1979, Nixon and Young, 2003) were then used to test against lobe-dependent tractography. (4) Probabilistic tractography data, pairwise connections and the corresponding $\log_{10}$-transfered connectivity strength index, *Cs*, were then used to generate a brain-wide neural connectivity matrix.

Construction of structural neural connectivity matrix

Imposing neuro-anatomical knowledge (e.g. trajectory of tracts of interest) to eliminate false positives leads to accurate reconstruction of the local fiber architecture and lobe-to-lobe connectivity. It indicates an optimized FOD amplitude cut-off value of 0.175 to generate biologically realistic tractography at mesoscale (see Figures 5A, 7-8, S2). It is worth noting that the tracking termination threshold (0.175) used in this study is highly conservative in contrast to the conventional value (0.01-0.1) applied previously in mouse (Smith et al., 2012, Liu et al., 2016). We then use the identical probabilistic algorithm and the optimized parameters to establish a brain-wide squid neural connectivity matrix where the connections and the corresponding connectivity strength (*Cs*) were mapped to the relevant squid brain lobes for each individual. The averaged pairwise *Cs* and the corresponding standard deviation were also calculated and plotted in the matrices for further analysis.

Proposing previously unknown lobe-to-lobe neural tracts

Another advantage of probabilistic tractography is capable of dealing with uncertainty in estimates of local fiber orientation and tracking non-dominant fiber populations, especially at the very high resolution obtained here using 16.4 T MRI (see detail discussion in (Behrens et al., 2007, Descoteaux et al., 2009)). This approach therefore allows estimation of probability of streamlines from each voxel and indicates previously invisible tracts not noticed due to the methodological constraint of classical histology. Furthermore, manipulating 3D predictive

tractography, such as highlighting the tracts of interest and identifying neighbour lobes close to the tracts, obtains an organizational reference to accurately guide invasive histological approaches, leading NeuroVue dyes being loaded in the target tracts to test and underpin both known and undescribed neural pathways.

In order to visualize the predictive new pathways on the connectivity matrix, the new lobe-to-lobe tracts and their distribution pattern are visualized against the known 282 tracts and are subtracted from all tracts recovered by the selected high value of *Cs* (2.7) (see Figure 5C).

Subdivisions of the basal lobe system and the corresponding neural connection atlas

Adding resolution parameters (e.g. sub-sectioning ROIs within a lobe) we can further reveal the network structure and the different spatial scales within the squid neural network. The parcellation-based approach has been broadly applied to investigate and subdivide specific brain areas in both structural and functional networks (Betzel and Bassett, 2017). Here we adopt this concept in order to define clearly the basal lobe system. The right half of the basal lobe system was further divided into 604 same sized small ROIs (each ROI voxel = 120μm x 120μm x 120μm) and these ROIs were evenly distributed across this system throughout the dorso-ventral axis (16 levels) (see Figure 6). The identical probabilistic algorithm and the optimised parameters established in this study were used to examine all 604 ROIs and render the corresponding tractography of the subdivided regions.

Supplemental References

ABBOTT, N. J., BUNDGAARD, M. & CSERR, H. F. 1985. Brain vascular volume, electrolytes and blood-brain interface in the cuttlefish *Sepia officinalis* (Cephalopoda). *J Physiol,* 368**,** 197-212.

BEHRENS, T. E., BERG, H. J., JBABDI, S., RUSHWORTH, M. F. & WOOLRICH, M. W. 2007. Probabilistic diffusion tractography with multiple fibre orientations: What can we gain? *Neuroimage,* 34**,** 144-155.

BETZEL, R. F. & BASSETT, D. S. 2017. Multi-scale brain networks. *NeuroImage,* 160**,** 73-83.

CAJAL, S. R. 1917. *Contribucion al conocimiento de la retina y centros opticos de los cefalopodos. Tarbajos del laboratorio de investigacious biologicas de la universidad de Madrid* Madrid.

CALAMANTE, F., TOURNIER, J. D., KURNIAWAN, N. D., YANG, Z., GYENGESI, E., GALLOWAY, G. J., REUTENS, D. C. & CONNELLY, A. 2012. Super-resolution track-density imaging studies of mouse brain: comparison to histology. *Neuroimage,* 59**,** 286-96.

CHUNG, W.-S. & MARSHALL, N. J. 2017. Complex visual adaptations in squid for specific tasks in different environments. *Front Physiol,* 8**,** 105.

DESCOTEAUX, M., DERICHE, R., KNOSCHE, T. R. & ANWANDER, A. 2009. Deterministic and probabilistic tractography based on complex fibre orientation distributions. *IEEE Trans Med Imaging,* 28**,** 269-86.

GIRARD, G., WHITTINGSTALL, K., DERICHE, R. & DESCOTEAUX, M. 2014. Towards quantitative connectivity analysis: reducing tractography biases. *Neuroimage,* 98**,** 266-78.
KOBAYASHI, S., TAKAYAMA, C. & IKEDA, Y. 2013. Ontogeny of the brain in oval squid *Sepioteuthis lessoniana* (Cephalopoda: Loliginidae) during the post-hatching phase. *J Mar Biol Assoc UK,* 93**,** 1663-1671.
KOIZUMI, M., SHIGENO, S., MIZUNAMI, M. & TANAKA, N. K. 2016. Three-dimensional brain atlas of pygmy squid, *Idiosepius paradoxus*, revealing the largest relative vertical lobe system volume among the cephalopods. *J Comp Neurol,* 524**,** 2142-2157.
LIU, C. R., LI, Y. H., EDWARDS, T. J., KURNIAWAN, N. D., RICHARDS, L. J. & JIANG, T. Z. 2016. Altered structural connectome in adolescent socially isolated mice. *Neuroimage,* 139**,** 259-270.
MESSENGER, J. B. 1979. The nervous system of *Loligo*. IV. Peduncle and olfactory lobes. *Philos Trans R Soc Lond B Biol Sci,* 285**,** 275-309.
NIXON, M. & YOUNG, J. Z. 2003. *The brains and lives of cephalopods,* Oxford, Oxford University Press.
SCHINDELIN, J., ARGANDA-CARRERAS, I., FRISE, E., KAYNIG, V., LONGAIR, M., PIETZSCH, T., PREIBISCH, S., RUEDEN, C., SAALFELD, S., SCHMID, B., TINEVEZ, J.-Y., WHITE, D. J., HARTENSTEIN, V., ELICEIRI, K., TOMANCAK, P. & CARDONA, A. 2012. Fiji: an open-source platform for biological-image analysis. *Nature Methods,* 9**,** 676.
SHIGENO, S., TSUCHIYA, K. & SEGAWA, S. 2001. Embryonic and paralarval development of the central nervous system of the loliginid squid *Sepioteuthis lessoniana*. *J Comp Neurol,* 437**,** 449-475.
SMITH, R. E., TOURNIER, J. D., CALAMANTE, F. & CONNELLY, A. 2012. Anatomically-constrained tractography: improved diffusion MRI streamlines tractography through effective use of anatomical information. *Neuroimage,* 62**,** 1924-1938.
STRAUSFELD, N. J. 1980. The Golgi method: Its application to the insect nervous system and the phenomenon of stochastic impregnation. *In:* STRAUSFELD, N. J. & MILLER, T. A. (eds.) *Neuroanatomical Techniques.* Springer New York.
TOURNIER, J. D., CALAMANTE, F. & CONNELLY, A. 2007. Robust determination of the fibre orientation distribution in diffusion MRI: non-negativity constrained super-resolved spherical deconvolution. *Neuroimage,* 35**,** 1459-72.
TOURNIER, J. D., CALAMANTE, F. & CONNELLY, A. 2012. Mrtrix: Diffusion tractography in crossing fiber regions. *Int J Imag Syst Tech,* 22**,** 53-66.
WILD, E., WOLLESEN, T., HASZPRUNAR, G. & HESS, M. 2015. Comparative 3D microanatomy and histology of the eyes and central nervous systems in coleoid cephalopod hatchlings. *Org Divers Evol,* 15**,** 37-64.
YOUNG, J. Z. 1974. The central nervous system of *Loligo*. I. The optic lobe. *Philos Trans R Soc Lond B Biol Sci,* 267**,** 263-302.
YOUNG, J. Z. 1976. The nervous system of *Loligo*. II. Subesophageal centers. *Philos Trans R Soc Lond B Biol Sci,* 274**,** 101-167.
YOUNG, J. Z. 1977. The nervous system of *Loligo*. III. Higher motor centers - The basal supraesophageal lobes. *Philos Trans R Soc Lond B Biol Sci,* 276**,** 351-398.
YOUNG, J. Z. 1979. The nervous system of *Loligo*. V. The vertical lobe complex. *Philos Trans R Soc Lond B Biol Sci,* 285**,** 311-354.
YUSHKEVICH, P. A., PIVEN, J., HAZLETT, H. C., SMITH, R. G., HO, S., GEE, J. C. & GERIG, G. 2006. User-guided 3D active contour segmentation of anatomical structures: Significantly improved efficiency and reliability. *NeuroImage,* 31**,** 1116-1128.